

3D thermal history and maturity modelling of the Levant Basin and its eastern margin, offshore–onshore Lebanon

Samer Bou Daher¹ · Mathieu Ducros² · Pauline Michel³ · Nicolas Hawie⁴ · Fadi H. Nader² · Ralf Littke¹

Received: 13 August 2015 / Accepted: 30 March 2016 / Published online: 17 May 2016
© Saudi Society for Geosciences 2016

Abstract In the last decade, the East Mediterranean Levant Basin has become a frontier hydrocarbon province. Several gas discoveries have been recorded in Miocene reservoirs offshore Israel, and seismic data suggest promising prospective plays in deeper intervals throughout the basin. Source rock quality, quantity, and distribution as well as thermal history are hitherto not well constrained, especially in the deep offshore. In this study, we present new source rock information from Jurassic to Paleocene intervals that prove the presence of several gas-prone and oil-prone potential source rocks along the eastern margin of the Levant Basin onshore Lebanon. None of the analysed onshore source rocks have reached sufficient thermal maturity for oil generation. However, 3D thermal history and maturity modelling indicate that these source rocks have reached thermal maturity in the offshore basin. Several potential petroleum systems have been suggested, including an Upper Cretaceous–Oligo-Miocene biogenic and thermogenic system in the deep basin, a Jurassic–Cretaceous system along the margin, and a Permian–Triassic system in the onshore. Sensitivity analysis in the poorly calibrated

offshore basin showed a large uncertainty with respect to the depth of the oil and gas window and suggested an important effect of the depth of the lithospheric–asthenospheric boundary on the thermal history of the basin. The different scenarios tested in this study showed that the thickness of the biogenic zone below the Messinian salt would vary between 700 and 1500 m in the deep basin offshore Lebanon.

Keywords Levant Basin · Petroleum systems · Basin modelling · Source rocks · Kinetics

Introduction

The growing global demand for oil, natural gas, and other sources of energy has moved exploration to challenging and complex provinces. The East Mediterranean region is one of those frontier provinces. Recent gas discoveries in Oligocene and Miocene sandstone reservoirs offshore Israel and Cyprus (e.g. Zohr, Tamar, Dalit, Leviathan, Karish, Tanin, Dolphin, and Cyprus-A) (www.nobleenergyinc.com; Esestime et al. 2016) have proven the hydrocarbon potential of the Levant Basin. The source of this gas is still unclear, although it has been reported to be of biogenic origin comprising 99 % methane (Needham et al. 2013). Oil discoveries in Mesozoic structures off the coast of Israel were also recorded in drilling campaigns during the 1990s (Gardosh 2013). Additionally, new seismic data acquired in the last decade revealed the large thickness of the sedimentary column and the presence of direct hydrocarbon indicators (DHI), thus suggesting the presence of working thermogenic petroleum systems rendering the under-explored Levant Basin one of the most promising hydrocarbon provinces in the region.

Onshore, the Palmyra Basin in Syria produces oil and gas from Early Cretaceous and Middle Triassic reservoirs,

✉ Samer Bou Daher
samer.boudaher@emr.rwth-aachen.de

¹ Energy and Mineral Resources Group (EMR), Institute of Geology and Geochemistry of Petroleum and Coal, RWTH Aachen University, Lochnerstrasse 4-20, 52056 Aachen, Germany

² Geology Department, Geosciences Division IFP Energies Nouvelles, 1&4 Av. de Bois-Préau, 92852 Rueil-Malmaison Cedex, France

³ Geochemistry-Petrophysics Department, Geosciences Division IFP Energies Nouvelles, 1 & 4 Av. de Bois-Préau, 92852 Rueil-Malmaison Cedex, France

⁴ Beicip-Franlab, 232 avenue Napoleon Bonaparte, 92500 Rueil-Malmaison, France

respectively (Nader 2014). Gas production is also ongoing from Carboniferous sandstone (Markada Formation) in several fields onshore Syria (Lučić et al. 2003). In Lebanon, seven exploration wells have been drilled between 1947 and 1966 penetrating only down to the Upper Jurassic which is the oldest surface-exposed rock formation. Drilling failed to encounter commercial oil and gas volumes in Lebanon, probably due to (i) meteoric water washing affecting the Jurassic and post-Jurassic rock succession and (ii) off structure position of drilled wells (Nader 2014). The pre-Jurassic succession might, however, include a working petroleum system similar to the Triassic petroleum system in Syria and sealed by the Kurrachine evaporites presumed to be present in Lebanon (Beydoun and Habib 1995; Brew et al. 2001; Nader 2014). These sediments are thought to be the extension of the Upper Triassic evaporites known in the Palmyra Basin (Renouard 1955; Beydoun and Habib 1995; Brew et al. 2001; Nader 2014).

The East Mediterranean offshore, onshore, and intermediate margin seem to include several promising petroleum systems. The thermal history of the region, as well as the distribution, quality, and maturity of major source rocks, is yet unknown. Thus, we constructed a 3D thermal history model (TemisFlow™, v. 2013.2) covering an area of 315×315 km (grid resolution 5×5 km) including the Levant Basin, margin, and onshore. New source rocks' kinetic data were produced and used in the model in order to assess the maturity and the timing of hydrocarbon generation of major source rocks and to discuss the implications on potential thermogenic petroleum systems in the study area.

Geological setting

An extensional rift phase along the northern margin of Gondwana started in the late Paleozoic and resulted in the formation of the Levant and the Palmyra basins (Fig. 1) (Garfunkel 1989; Hawie et al. 2013a; Montadert et al. 2014; Nader 2014). Successive rift pulses affected the Levant Basin until the Late Jurassic (Gardosh et al. 2010; Hawie et al. 2013a). A calm post-rift cooling and subsidence phase prevailed until the Late Cretaceous (Hawie et al. 2013a). In the Palmyra Basin, subsidence started in the Late Permian and continued till the Late Cretaceous (Ponikarov 1966; Chaimov et al. 1992). During the Late Cretaceous, the closure of the Neotethys Ocean and the collision of the Afro-Arabian and Eurasian plates started. The compressional regime persisted until the Miocene leading to the emplacement of the Syrian Arc fold belt and the inversion of Mesozoic extensional structures in the Palmyra Basin (Ponikarov 1966; Chaimov et al. 1992; Robertson 1998; Walley 1998). The two major phases of Syrian Arc folding occurred in the Coniacian (Late Cretaceous) and Late Eocene (Garfunkel 1998; Walley

1998). The initiation of the Red Sea rifting during the Oligocene/Miocene resulted in the propagation of a series of strike-slip faults northward forming the Levant Fracture System which extends from the Gulf of Aqaba to the Taurus Mountains (Beydoun 1999). The Levant Fracture System is a sinistral fault system that includes the N–S striking Dead Sea segment, the NNE–SSW central segment (Yammounh Fault and fault splays) forming a restraining bend in Lebanon, and the N–S Ghab Fault segment (Ghalayini et al. 2014).

Lithostratigraphic framework

The onshore Jurassic–Quaternary stratigraphy was constrained based on field investigations and biostratigraphic studies (Müller et al. 2010; Hawie et al. 2013b; Nader 2014; Bou Daher et al. 2015). The offshore Jurassic–Quaternary stratigraphy was postulated mostly based on seismic interpretation (Hawie et al. 2013a). The pre-Jurassic stratigraphy was inferred from regional correlations based on published data from neighbouring countries (Brew et al. 2001; Nader 2003; Gardosh et al. 2008; Naylor et al. 2013).

The Mesozoic lithostratigraphic succession of the Levant Basin and that of onshore Lebanon realm are relatively similar and mostly dominated by carbonates (Fig. 2) (Nader 2014). In the late Cretaceous, the Afro-Arabian and Eurasian plate convergence and the emplacement of a flexural basin resulted in differential subsidence and deposition of hemipelagic/pelagic and clastic Neogene basinal fill while the marginal realms remained predominated by carbonate platforms (Fig. 2) (Hawie et al. 2013a&b). Sedimentation in the basin was almost uninterrupted while in the margin and onshore several erosion events are recorded (Müller et al. 2010; Hawie et al. 2013b). The latest ongoing erosion event is related to the uplift of Mount Lebanon and Anti-Lebanon, reaching its acme during the middle/late Miocene as a result of a transpressive regime at the Lebanese segment of the Levant Fracture System (Beydoun 1999; Gomez et al. 2006, Hawie et al. 2013a). This event led to the exposure of the Jurassic cores of the Lebanese mountains while deposition continued in the adjacent topographic lows, e.g. Bekaa Valley and the coastal areas (Fig. 1) (Khair et al. 1997; Hawie et al. 2013a; Nader 2014). The erosional thicknesses were estimated based on regional correlations and on maturity data when available (Fig. 2) (Brew et al. 2001; Nader 2003; Gardosh et al. 2008; Naylor et al. 2013).

Several volcanic episodes are recorded along the eastern margin of the Levant Basin (Fig. 2). Late Jurassic–Early Cretaceous alkaline volcanism is found in north Lebanon and completely absent in south Lebanon (Dubretret 1955; Nader 2014). Wilson (1992) and Garfunkel (1992) attributed this regional intermittent volcanism to mantle plume activity in the Levant region. Another episode of volcanism occurred in the late Cenozoic (Fig. 2). These alkaline volcanics are

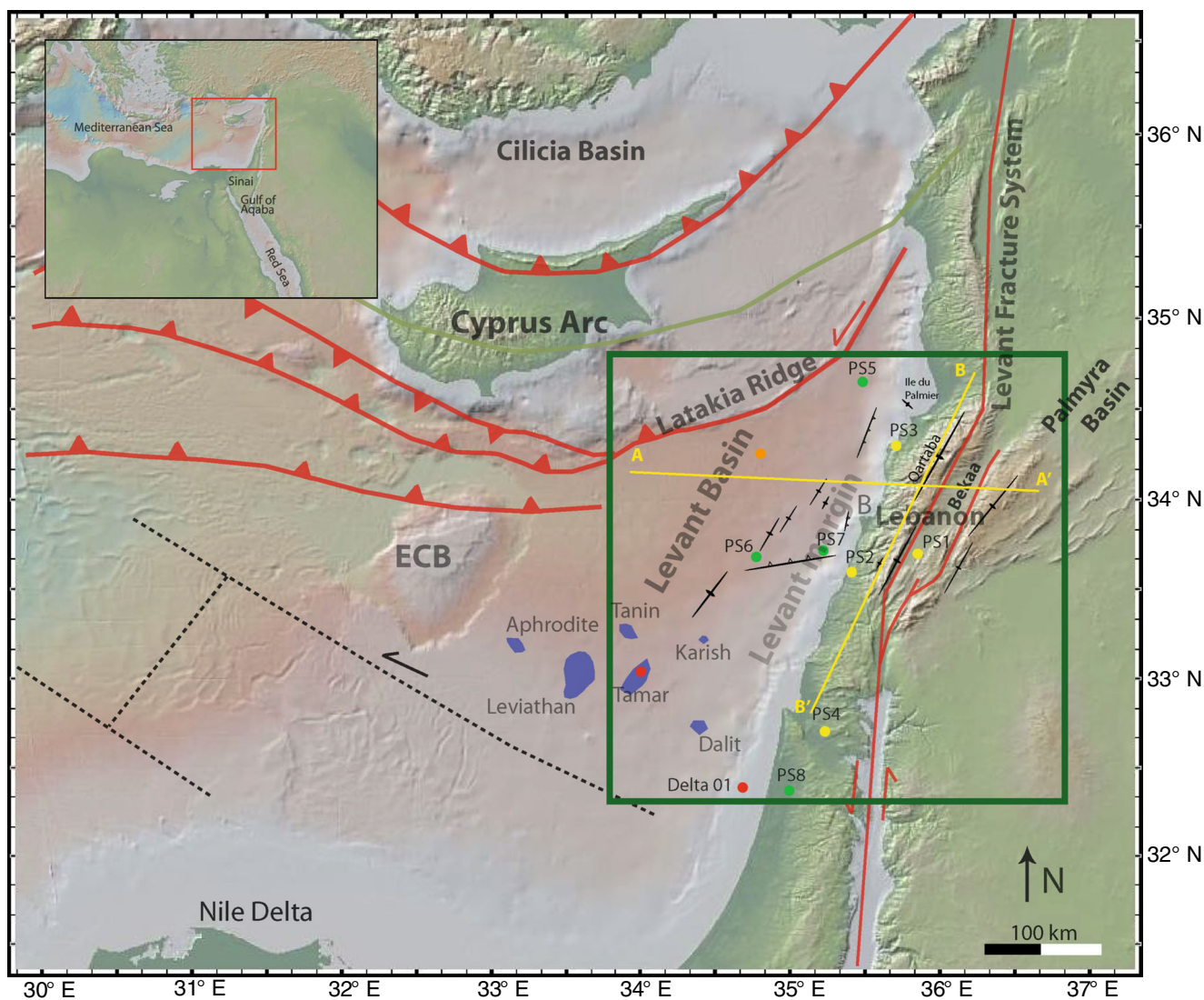


Fig. 1 Regional map of the east Mediterranean showing major structural elements. *Green square* marks the modelled area. PS1–PS8 are pseudo wells created for calibration, yellow pseudo wells have vitrinite reflectance data, and green pseudo wells have temperature data. *Orange*

circle marks the position of 1D extract reported in Figs. 11 and 12. (Modified after Hawie et al. 2013a; Bou Daher et al. 2014; Ghalayini et al. 2014)

linked to open cracks related to the Levant Fracture System permitting local deep decompression and magma ascent (Adiyaman and Chorowicz 2002). Abdel-Rahman and Nassar (2004) attributed the Pliocene alkali basalts of northern Lebanon to a transtensional regime at the junction of the Lebanese restraining bend and the Ghab segment of the Levant Fracture System.

Materials and methods

Source rocks

Twenty-six samples were collected from potential source rock intervals within the Kimmeridgian, Neocomian (Lower

Cretaceous), Albian, Cenomanian, and Upper Paleocene in different outcrops and shallow boreholes onshore Lebanon. TOC, TIC, and Rock-Eval pyrolysis were performed on all samples using a *LiquiTOC II* and a *Rock-Eval VI* device, respectively. Additionally, Campanian–lower Maastrichtian Rock-Eval data is taken from Bou Daher et al. (2014, 2015). Total sulphur (TS) content was measured using a Leco S200 analyzer (detection limit 20 ppm; error < 5 %).

Vitrinite reflectance measurements were conducted on nine Neocomian coaly shales and two Cenomanian calcareous shales. Sample cuttings were prepared according to guidelines described by Taylor et al. (1998). Random vitrinite reflectance was measured at a magnification of ×500 in a dark room with a *Zeiss Axio Imager* microscope for incident light equipped with a tungsten–

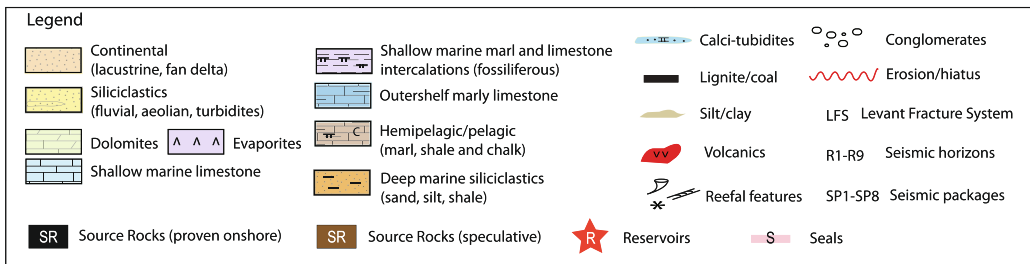
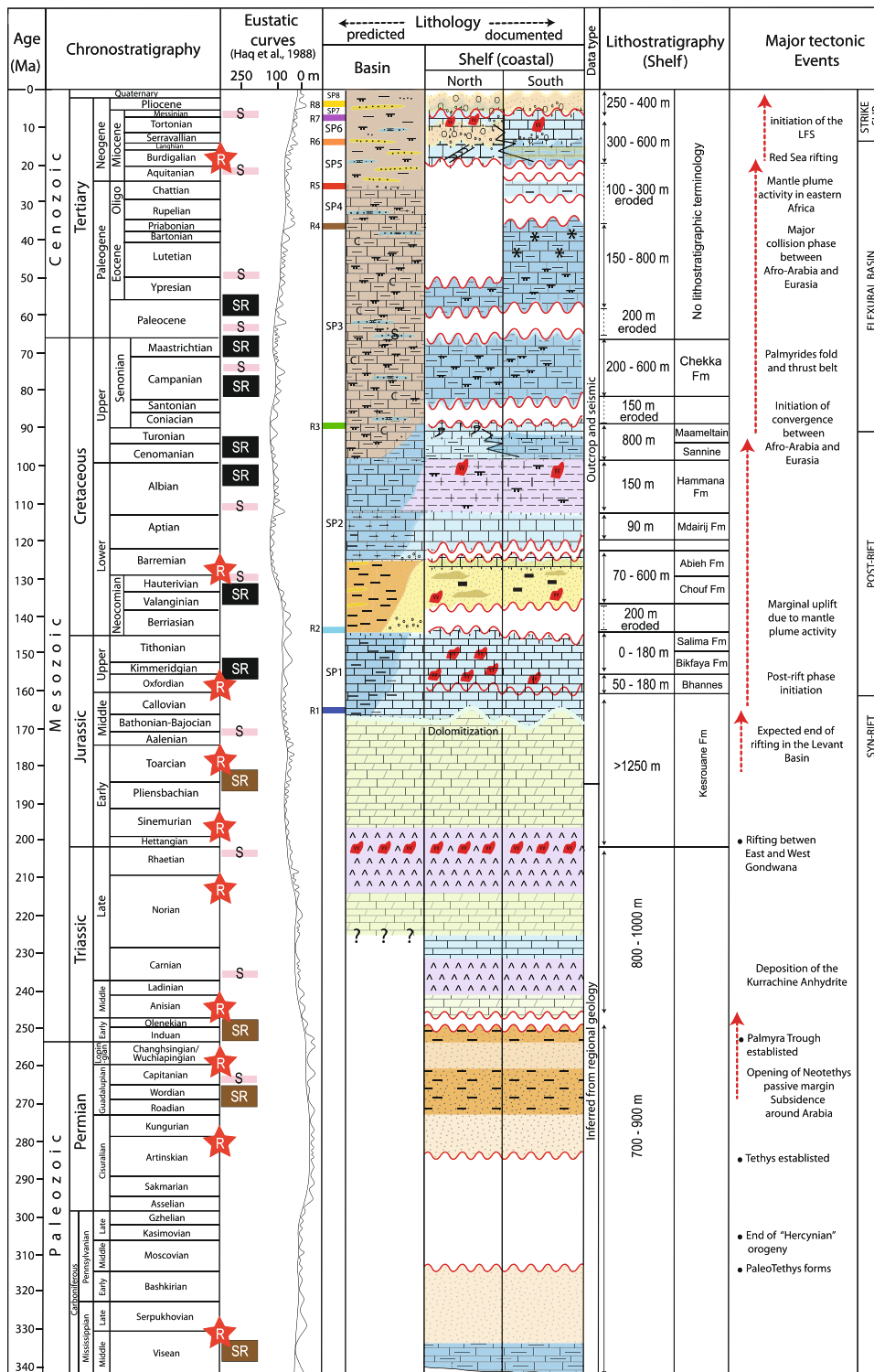


Fig. 2 Stratigraphic chart showing the onshore sedimentary facies and their extrapolation into the offshore basin, the main petroleum system elements, and the major tectonic events (modified after Hawie et al. 2013a)

halogen lamp (12 V, 100 W), a 50X/0.85 *Epiplan-NEOFLUAR* oil immersion objective, and a 546-nm filter and using *Zeiss* immersion oil with refraction index $n = 1.518$; 23 °C. For calibration, a leuco-sapphire mineral standard (0.592 %) was used. Details of sample preparation and microscopic equipment are described in Littke et al. (2012). Vitrinite reflectance data for the Campanian rocks was taken from Bou Daher et al. (2014, 2015).

Bulk hydrocarbon generation kinetics were determined for five samples. Kerogen was isolated from the samples by

elimination of minerals using non-oxidizing acid treatment under a continuous nitrogen flow (Durand and Nicaise 1980; Behar et al. 2008), followed by a soxhlet extraction for 1 h using DCM to eliminate the bitumen fraction. A Rock-Eval VI apparatus was used to conduct the experiments. A pyrolysis run was realized on a portion of each sample to ensure that the S1 peak was successfully eliminated. XRD analysis was also performed prior and post-acid treatment to insure the elimination of mineral matter. Bulk hydrocarbon generation rates were then measured at five different heating rates (2, 5, 10, 15, 25 °C/min) starting at 200 °C for 15 min and reaching to 700 °C.

The bulk hydrocarbon generation curves were then used to calculate mean activation energy (E_a) and a pre-exponential factor (A) for every sample using the least squares method according to Schenk et al. (1997). A discrete model with a

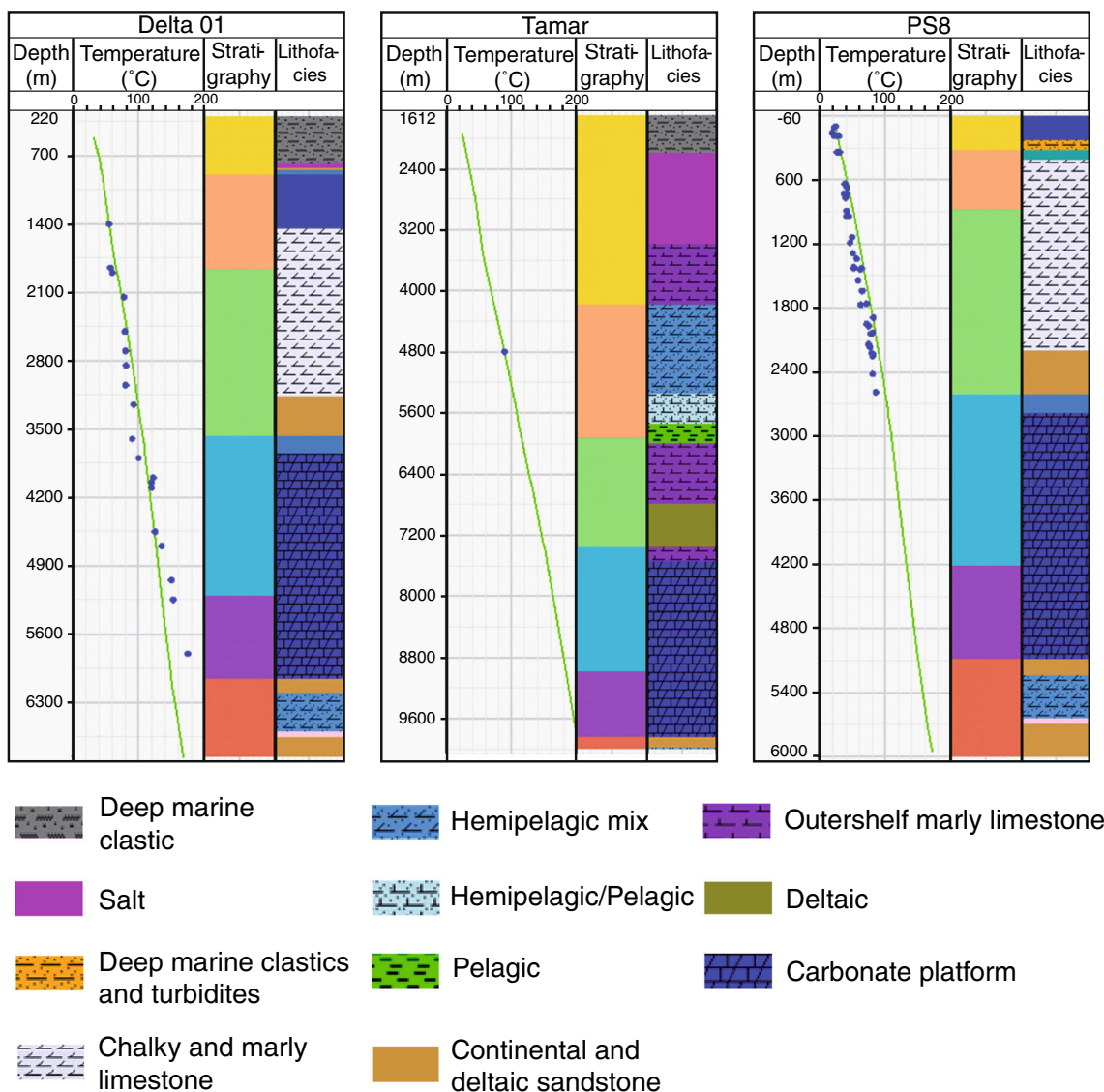


Fig. 3 a Temperature calibration in wells Delta 01 and Tamar, and pseudo well PS8. b Vitrinite reflectance calibration in pseudo wells (see Fig. 1 for location). Colour-coded stratigraphy based on international chronostratigraphic chart

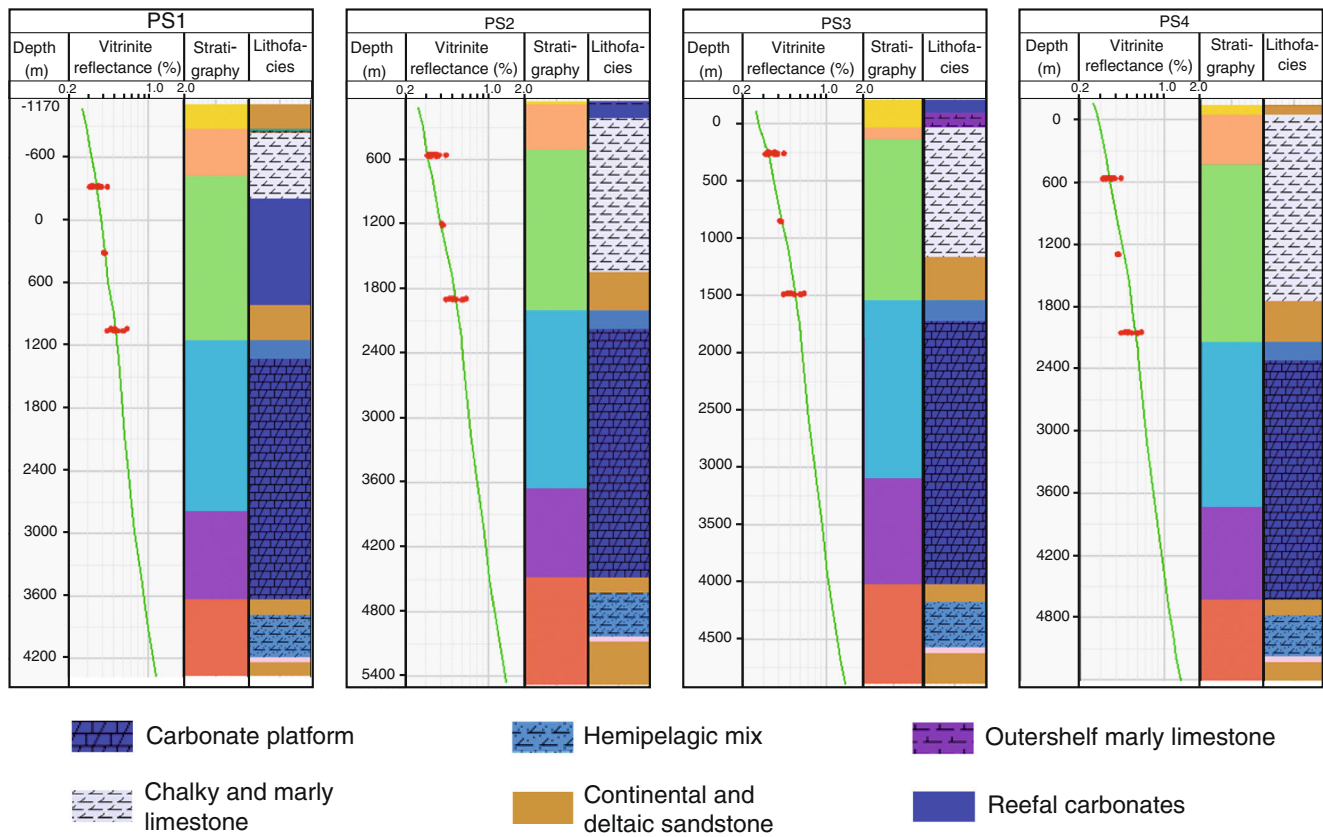


Fig. 3 (continued).

spacing of 2 kcal/mol between consecutive activation energies was adopted, and an IFPEN software, *GeoKin*, was used to calculate the activation energy distributions using the previously calculated pre-exponential factor (A).

3D data set

Regional isopach maps for the Levant Basin and margin representing the Jurassic to Plio-Quaternary units were provided by Hawie (2014) who constructed the maps based on available literature (Ponikarov 1966; Ukla 1970; Dubertret 1975; Brew et al. 2001; Hardenberg and Robertson 2007; Gardosh et al. 2008; Powell and Moh'd 2011; Zilberman and Calvo 2013; Hawie et al. 2013a&b). The thicknesses of the pre-Jurassic units were also inferred from data published in neighbouring countries (Brew et al. 2001; Nader 2003; Gardosh et al. 2008; Naylor et al. 2013). However, for simplicity, constant values as shown in Fig. 2 were used for the pre-Jurassic units, except where specific data was available.

Lithological information was based on published data (e.g. Dubertret 1975; Saint-Marc 1972, 1974; BouBou Dagher-Fadel and Clark 2006; Gardosh et al. 2008; Bowman 2011; Hawie et al. 2013a&b) according to the lithostratigraphic framework illustrated in Fig. 2.

Bathymetry maps were defined using sedimentological and biostratigraphical investigation in the onshore and seismically interpreted in the offshore (Hawie et al. 2013a&b; Hawie 2014).

Boundary conditions

As an upper thermal boundary, the bottom water temperature (for the offshore) and the surface temperature (for the onshore) and its evolution through the basin history was derived from Wygrala (1989). The lower boundary condition and its evolution through time were determined using a McKenzie-type crustal model with the *TemisFlow*TM "Advanced basement" tool. This crustal model was constructed based on the assumption that the crust flooring the Levant basin is attenuated continental rather than oceanic (Beydoun 1977; Khair et al. 1993, 1997; Makris et al. 1983; Netzeband et al. 2006; Segev et al. 2006). Present-day crustal thicknesses were set to 8 km under the basin's central axis and 24 km under the onshore realm based on seismic refraction data presented in Netzeband et al. (2006). The depth of the lithospheric–asthenospheric boundary (LAB) with the thermal value of 1333 °C was adjusted to provide a best fit with the available calibration data and was set at

Table 1 Summary of source rocks data gathered from onshore Lebanon

| Sample # | Age | TOC (wt.%) | TIC (wt.%) | TS (wt.%) | SI (mg/g rock) | S2 (mg/g rock) | S3 (mg/g rock) | HI (mgHC/g TOC) | OI (mg CO2/g TOC) | PI (S1/(S1 + S2)) | Tmax (°C) | VRr (%) | GPS |
|----------------|-----------------|------------|------------|-----------|----------------|----------------|----------------|-----------------|-------------------|-------------------|-----------|-------------------------------|--------------------------------------|
| 1 | Upper Paleocene | 0.9 | 8.6 | 0.7 | 0.09 | 4.00 | 1.32 | 444 | 146 | 0.02 | 424 | - | N 34° 19' 47.65" E 35° 45' 49.19" |
| 2 | Upper Paleocene | 0.8 | 7.1 | 0.5 | 0.07 | 2.95 | 1.22 | 361 | 150 | 0.02 | 433 | - | N 34° 19' 47.65" E 35° 45' 49.19" |
| 3 | Upper Paleocene | 1.3 | 9.1 | 0.7 | 0.06 | 6.38 | 1.21 | 508 | 96 | 0.01 | 430 | - | N 34° 19' 47.65" E 35° 45' 49.19" |
| 4 | Upper Paleocene | 1.4 | 7.6 | 0.8 | 0.05 | 6.17 | 1.31 | 450 | 96 | 0.01 | 428 | - | N 34° 19' 47.65" E 35° 45' 49.19" |
| 5 ^a | Upper Paleocene | 1.3 | 7.1 | 0.7 | 0.05 | 3.24 | 1.88 | 245 | 142 | 0.02 | 426 | - | N 34° 19' 47.65" E 35° 45' 49.19" |
| 6 | Upper Paleocene | 1.0 | 7.3 | 1.0 | 0.05 | 3.09 | 1.31 | 319 | 135 | 0.01 | 431 | - | N 34° 19' 47.65" E 35° 45' 49.19" |
| 7 | Upper Paleocene | 1.0 | 7.6 | 1.0 | 0.04 | 3.44 | 1.21 | 355 | 125 | 0.01 | 431 | - | N 34° 19' 47.65" E 35° 45' 49.19" |
| 8 | Upper Paleocene | 0.5 | 9.1 | 0.5 | 0.03 | 1.21 | 1.25 | 235 | 244 | 0.02 | 431 | - | N 34° 19' 47.65" E 35° 45' 49.19" |
| 9 | Upper Paleocene | 0.5 | 8.7 | 0.9 | 0.03 | 0.75 | 1.18 | 154 | 242 | 0.04 | 424 | - | N 34° 19' 47.65" E 35° 45' 49.19" |
| 10 | Upper Paleocene | 0.5 | 7.9 | 1.3 | 0.04 | 0.49 | 1.22 | 100 | 249 | 0.07 | 416 | - | N 34° 19' 47.65" E 35° 45' 49.19" |
| 11 | Cenomanian | 1.2 | 12.8 | - | 0.14 | 10.68 | 1.16 | 890 | 97 | 0.01 | 405 | 0.41 (n = 16; s = 0.026) | N 34° 10' 04.86" E 35° 45' 25.10" |
| 12 | Cenomanian | 0.9 | 12.2 | - | 0.17 | 7.56 | 1.19 | 840 | 132 | 0.02 | 405 | 0.42 (n = 7; s = 0.032) | N 34° 10' 04.86" E 35° 45' 25.10" |
| 13 | Albian | 0.4 | 10.0 | - | 0.01 | 0.17 | 1.34 | 42 | 334 | 0.06 | 423 | - | N 33° 32' 05.84" E 35° 34' 51.23" |
| 14 | Albian | 0.5 | 5.8 | - | 0.04 | 0.42 | 1.27 | 83 | 254 | 0.09 | 416 | - | N 33° 32' 05.84" E 35° 34' 51.23" |
| 15 | Neocomian | 37.6 | 0.0 | 4.73 | 1.04 | 16.31 | 18.42 | 43 | 49 | 0.06 | 415 | 0.54 (n = 100; s = 0.059) | N 33° 37' 59.8" E 35° 55' 21.2" |
| 16 | Neocomian | 10.8 | 1.5 | 0.97 | 0.15 | 10.63 | 4.25 | 99 | 39 | 0.01 | 418 | 0.444 (n = 100; s = 0.039) | N 33° 33' 00.7" E 35° 33' 02.2" |
| 17 | Neocomian | 31.3 | 1.4 | 1.14 | 0.30 | 17.78 | 11.48 | 57 | 37 | 0.02 | 418 | 0.513 (n = 100; s = 0.055) | N 33° 33' 00.7" E 35° 33' 02.2" |
| 18 | Neocomian | 2.4 | 0.0 | 1.03 | 0.15 | 0.45 | 1.89 | 19 | 80 | 0.25 | 415 | 0.655 (n = 100; s = 0.051) | N 33° 33' 00.7" E 35° 33' 02.2" |
| 19 | Neocomian | 24.2 | 1.5 | 1.05 | 1.09 | 47.67 | 9.06 | 197 | 37 | 0.02 | 416 | 0.47 (n = 100; s = 0.057) | N 33° 33' 00.7" E 35° 33' 02.2" |

Table 1 (continued)

| Sample # | Age | TOC (wt.%) | TIC (wt.%) | TS (wt.%) | SI (mg/g rock) | S2 (mg/g rock) | S3 (mg/g rock) | HI (mgHC/g TOC) | OI (mg CO ₂ /g TOC) | PI (S1/(S1+S2)) | Tmax (°C) | VRr (%) | GPS |
|--|--------------|----------------|-------------------|-----------------|------------------|-------------------|------------------|-----------------|--------------------------------|-----------------|---------------|---|--------------------------------------|
| 20 | Neocomian | 8.3 | 1.3 | 0.34 | 0.19 | 5.10 | 4.60 | 61 | 55 | 0.04 | 423 | 0.481 (<i>n</i> = 100; <i>s</i> = 0.045) | N 33° 33' 00.7" E 35° 33' 02.2" |
| 21 | Neocomian | 0.3 | 0.2 | 0.10 | 0.03 | 0.27 | 1.12 | 81 | 335 | 0.10 | 429 | – | N 33° 36' 11.2" E 35° 38' 24.2" |
| 22 | Neocomian | 3.9 | 0.0 | 0.29 | 0.16 | 2.55 | 1.48 | 66 | 38 | 0.06 | 425 | – | N 33° 36' 11.2" E 35° 38' 24.2" |
| 23 | Neocomian | 14.0 | 0.0 | 1.76 | 0.34 | 5.16 | 13.33 | 37 | 95 | 0.06 | 429 | 0.608 (<i>n</i> = 100; <i>s</i> = 0.042) | N 33° 36' 11.2" E 35° 38' 24.2" |
| 24 | Neocomian | 62.0 | 0.0 | 5.24 | 1.48 | 79.56 | 31.83 | 128 | 51 | 0.02 | 415 | 0.603 (<i>n</i> = 100; <i>s</i> = 0.032) | N 34° 04' 06.2" E 35° 51' 10.3" |
| 25 ^a | Neocomian | 2.3 | 0.2 | 0.176 | 0.06 | 5 | 1.55 | 215 | 66 | 0.01 | 433 | 0.514 (<i>n</i> = 100; <i>s</i> = 0.078) | N 34° 04' 06.2" E 35° 51' 10.3" |
| 26 ^a | Kimmeridgian | 53.3 | 3.5 | – | 2.61 | 158.41 | 16.29 | 297 | 31 | 0.02 | 400 | – | N 33° 54' 28.5" E 35° 36' 23.6" |
| Campanian–lower Maastrichtian ^b | | 0.5–11.6 (3.8) | 3.65–12.76 (10.0) | 0.08–1.7 (0.79) | 0.04–7.67 (0.75) | 1.37–82.98 (25.8) | 0.85–4.92 (1.78) | 257–872 (559) | 22–242 (63) | 0.01–0.1 (0.02) | 405–434 (422) | 0.31–0.44 (0.35) | |
| Campanian 1 ^a | | 1.9 | 10.8 | 0.59 | 0.11 | 10.36 | 1.32 | 542 | 69 | 0.01 | 427 | 0.33 (<i>n</i> = 33; <i>s</i> = 0.072) | N 34° 19' 46.90" E 35° 45' 21.83" |
| Campanian 2 ^a | | 7.5 | 9.4 | 1.2 | 0.67 | 54.50 | 1.74 | 725 | 23 | 0.01 | 411 | 0.33 (<i>n</i> = 29; <i>s</i> = 0.026) | N 33° 24' 13.16" E 35° 39' 44.91" |

^a Sample selected for kinetic experiments^b Data from Bou Daher et al. 2014 and 2015)

90 km under the stretched continental crust in the basin and 115 km under the onshore. Pre-rift crustal thickness was assumed to be 24 km. Thus, a Beta factor map was calculated and three rifting events were introduced in the Permian, Triassic, and Early Jurassic. The heat flow (HF) at the base of the sediments was then produced as an output of the crustal model.

Vitrinite reflectance and transformation ratio

The calculation of vitrinite reflectance was based on the EASY Ro% kinetic after Sweeney and Burnham (1990). Transformation ratios were calculated using the measured kinetics for each reported source rock and using the following formula:

$$\text{Transformation Ratio}\% = \frac{(\text{Initial HC Potential} - \text{Current HC Potential}) \times 100}{\text{Initial HC Potential}}$$

Results and discussion

Calibration

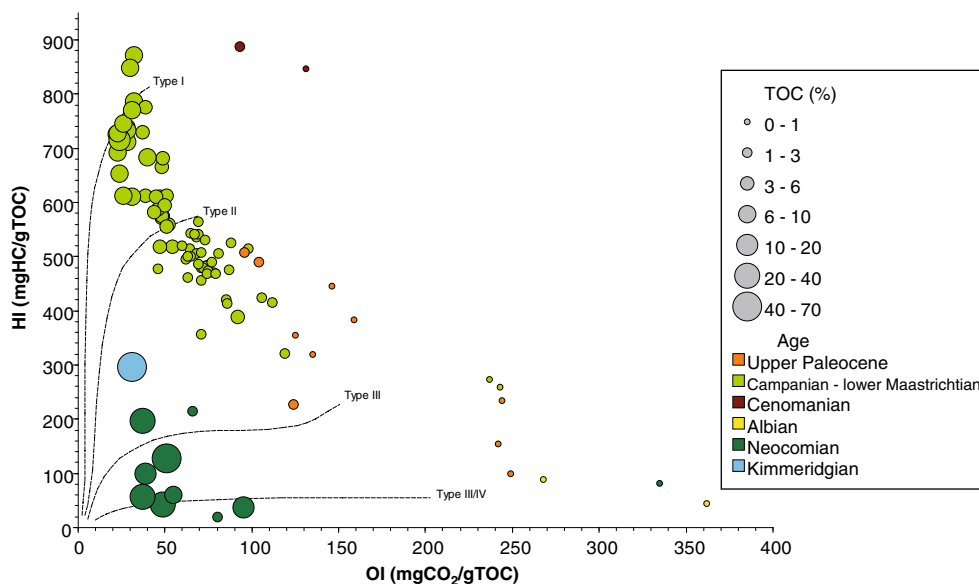
Calibration data used in this study consists of borehole temperature data and vitrinite reflectance data (Fig. 3a, b). Temperature data for Delta 01 and Tamar wells was derived from Dubille and Thomas (2012). Due to the scarcity of calibration points in many parts of the basin, especially the offshore, temperature data from calibration wells was used not only at the wells’ location but also for calibration in pseudo wells in areas of the basin with similar crustal thickness,

lithologies, salt thickness, and bathymetry to the location of the wells to which the calibration data belongs (Fig. 1). Temperature data from nearby Nir-Am field (SW-Israel) (Shalev et al. 2013) was similarly used for calibration in pseudo well PS8 (Fig. 1). Vitrinite reflectance data (Fig. 3b) was measured on outcrop and near-surface samples collected from Mount Lebanon (Table 1). 1D burial analysis showed that those rocks have reached their deepest burial during the middle Miocene while their adjacent equivalents in the Bekaa Valley and along the coastal areas have reached their deepest burial at the present day due to continuous sedimentation since the Miocene. However, the increase in the calculated VRr for all layers between the middle Miocene and present day is small where the Miocene–Quaternary rock succession is not of a great thickness (<300 m). Thus, the vitrinite reflectance data collected from Lower Cretaceous, Cenomanian, and Campanian rocks on and around Mount Lebanon were used for calibration in several pseudo wells (Fig. 1) where the Miocene–Quaternary rock succession is not thicker than 300 m (Fig. 3b). The use of surface-collected vitrinite reflectance data for calibration in pseudo wells is further explained in Noeth et al. (2001, 2002).

Source rocks

The Rock-Eval data (Table 1; Fig. 4) proved the presence of several oil-prone and gas-prone source rocks, with varying bulk hydrocarbon generation kinetics (Fig. 5), along the eastern margin of the Levant basin. The Paleocene contains around 30 m of calcareous source rocks showing a wide range of HI and OI values, varying from 100 to 508 mgHC/gTOC and from 96 to 249 mgCO₂/gTOC, respectively (Table 1; Fig. 4). The variation observed in HI and OI values of Paleocene source rocks can be due to changes in the relative

Fig. 4 Pseudo Van-Krevelen diagram showing the type and the organic content of the source rocks sampled onshore Lebanon



input of marine and terrestrial organic matter and/or due to oxidation of marine organic matter resulting in a kerogen type varying between types II and III. The Campanian–lower Maastrichtian contains around 150 m of calcareous source rocks that show a wide range of HI and OI values, varying from 257 to 872 mgHC/gTOC and from 22 to 242 mgCO₂/gTOC, respectively (Table 1; Fig. 4). The variation observed in the HI and OI values of the Campanian–lower Maastrichtian source rocks is most probably due to differences in bottom water redox conditions at the time of deposition (Bou Daher et al. 2014, 2015). The Campanian–lower Maastrichtian source rocks are of marine origin and plot in the types I and II field in Fig. 4. Detailed geochemical and petrographic results confirm the presence of type IIS kerogen

especially in the TOC-rich intervals of the Campanian–lower Maastrichtian source rocks (Bou Daher et al. 2015).

The Cenomanian includes also marine calcareous source rocks showing very high HI and relatively low OI values (Table 1; Fig. 4). The vertical extent of the Cenomanian source rocks in Lebanon is restricted to a few beds (3–4 m) only, but this source rock might have a larger extent in the offshore as it might be related to an ocean anoxic event (Kolonic et al. 2002; Lüning et al. 2004; Sachse et al. 2011). Similar Cenomanian source rock quality has been reported in the Bahriya formation of the western desert, Egypt (Moretti et al. 2010). The Albian source rock shows a poor quality (type III/IV kerogen) and a low TOC (Table 1; Fig. 4). The Neocomian (Lower Cretaceous) consists of coaly shales of moderate source rock

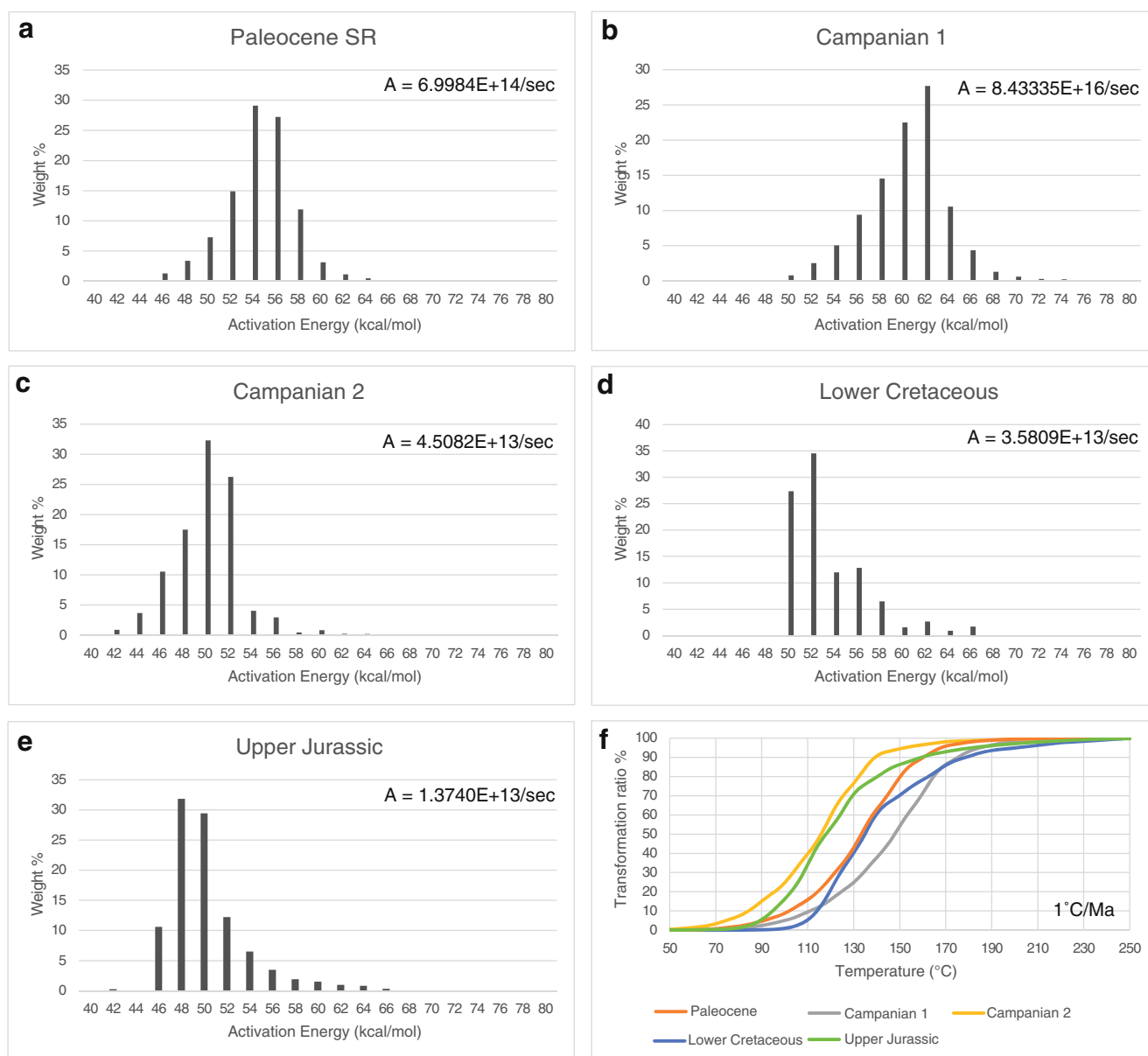


Fig. 5 a–e Bulk hydrocarbon generation kinetics of five source rock samples and f their calculated transformation ratio for a heating rate of 1 °C/Ma

quality (Table 1; Fig. 4) interbedded within the sandstones of the Chouf formation. This source rock seems to be of regional extent, as it is also reported in the Alam El Bueib formation of the western desert, Egypt (Moretti et al. 2010). The total thickness of the organic rich beds in the Neocomian onshore Lebanon can reach up to 12 m. Kimmeridgian source rocks onshore Lebanon consists of thin (<0.5 m) lenses of shales with very high TOC, moderate HI, and low OI within a generally reefal carbonate formation (Table 1; Fig. 4). However, very prolific Upper Jurassic source rocks are known to exist in the Middle East (Murriss 1980; Ayres et al. 1982). All the source rocks analysed from onshore Lebanon are immature (Table 1).

The activation energy distribution for the Paleocene source rock shows a typical type II bell-shaped distribution (Fig. 5a). The Campanian source rock shows a major difference in the activation energy distribution between Campanian 1 and Campanian 2 samples (Fig. 5b, c) which can be attributed to the presence of type II (Campanian 1) and type IIS (Campanian 2) kerogen. A depositional model for the Campanian–lower Maastrichtian source rocks was proposed by Bou Daher et al. (2015) suggesting that type II kerogen with high activation energies would be expected for the Campanian source rocks in the basin, while along most of the onshore type IIS kerogen with lower activation energies is more abundant. The Lower Cretaceous and Upper Jurassic coaly shales show a wide spectrum of activation energies tailing up to 66 kcal/mol which is observed in many type III kerogen bearing source rocks (Fig. 5d, e) (Schenk et al. 1997). The presence of these reported source rocks in the offshore part of the study area is an open question. However, molecular and isotopic data from gaseous hydrocarbons encountered in the Mesozoic–Cenozoic section at the continental margin offshore Israel suggest the presence of several genetic systems (Feinstein et al. 2002, 2013).

Heat flow

The modelled basal heat flow (HF) showed different trends in the basin, margin, and onshore areas (Fig. 6). In the basinal realm, an elevated HF during the Permian–Early Jurassic is the result of rifting pulses that occurred during that period. The HF values in the basin decrease slowly during the post-rift cooling and subsidence phase until the late Eocene/early Oligocene when a fast decrease in HF occurs, most probably as a result of fast sedimentation (Fig. 6a). Along the margin, the HF trend is relatively similar to the basinal area, but with lower calculated HF values for the Permian–Early Jurassic and slightly higher ones during the last 40 Ma (Fig. 6b), which is due to a lower β factor and a lower sedimentation rate along the margin, respectively. In the onshore area, our model shows relatively constant values through time, varying slightly above 50 mW/m² with an increase in the last 10 Ma due to uplift and

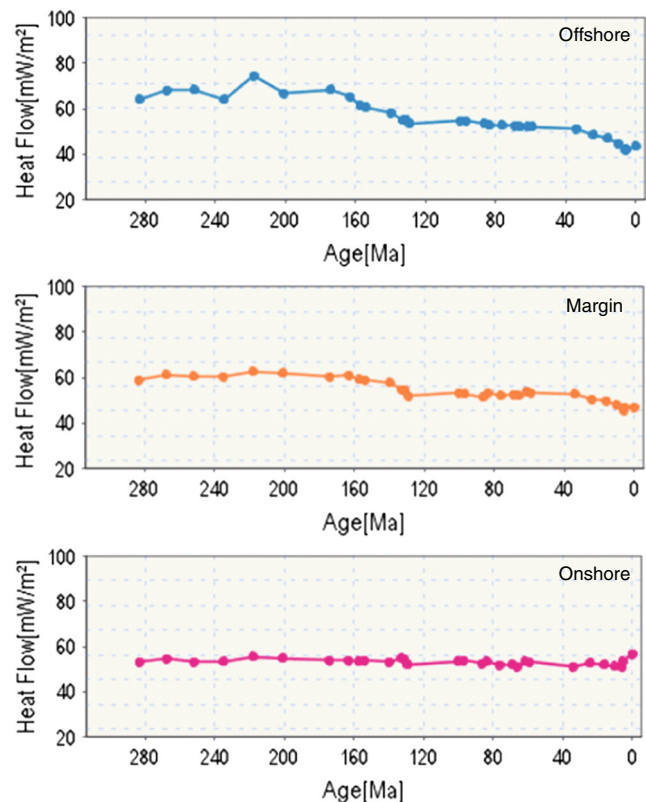


Fig. 6 Basal heat flow trends for the offshore basin, margin, and onshore Lebanon

erosion of Mount Lebanon (Fig. 6c). The modelled present-day HF in this study shows higher values in the onshore than in the offshore, which is in accordance with the few data available on the present-day surface heat flow. Jiménez-Munt et al. (2006) reported HF values ranging from 40 to 60 mW/m² with an increase from the thin continental crust flooring the basin to the thicker crust in the onshore. Makris and Stobbe (1984) also reported a similar trend from 0.9 HFU (38 mW/m²) in the basin to 1.6 HFU (67 mW/m²) in the onshore. Many other authors reported a similar decrease in the HF values from the onshore to the offshore as well as from the southern margin (southern Israel) northwards (northern Israel) (Eckstein and Simmons 1978; Roded et al. 2013; Shalev et al. 2013; Schütz et al. 2014). This trend is most probably the result of a decrease in the thickness of the radiogenic continental crust and an increase in the less radiogenic sedimentary cover. The resulting average present-day geothermal gradient varies from 19 °C/km in the offshore basin to around 25 °C/km in the onshore area.

Burial history and maturity

The different geodynamic events experienced by the Levant Basin and the onshore Levant region have been recorded differently in the sedimentary successions of different parts of the study area, particularly during the Cenozoic. Since the middle

Eocene, the northwestern part of the Arabian plate has been emerging out of the water (Bar et al. 2011), resulting in several regional erosion events (Hawie et al. 2013a), while the nearby Levant basin has been rapidly subsiding and accumulating more than 5 km of sediments (Hawie et al. 2013b). This differential vertical movement had an important effect on the thermal history and source rock maturity of the study area. To illustrate this effect, four burial history diagrams were extracted from four different areas of the model (Fig. 7). Up until the Late Cretaceous, the study area underwent a relatively similar burial history with only slightly higher thermal maturity in the offshore basin due to higher heat flow resulting from rifting pulses at that time.

The Cenozoic burial history, however, differs considerably in the onshore from the offshore (Fig. 7a–d). A fast

burial in the deep offshore basin during the last 60 Ma (Fig. 7a) resulted in the thermal maturation of all Mesozoic and early Cenozoic source rocks. A similar fast burial occurred along the margin, but with a shallower depth due to the thinner Neogene cover, resulting in the thermal maturation of most of the Mesozoic with the exception of the Upper Cretaceous (Fig. 7b). In the onshore, deepest burial on Mount Lebanon was reached in the middle Miocene leading to a halt in maturation since that time (Fig. 7c). In the Bekaa Valley and along the coastal area and topographic lows onshore, sedimentation continued during the uplift of Mount Lebanon throughout the Miocene, Pliocene, and Quaternary resulting in the deepest burial at the present day (Fig. 7d). With the exception of the Jurassic in the Bekaa Valley reaching the

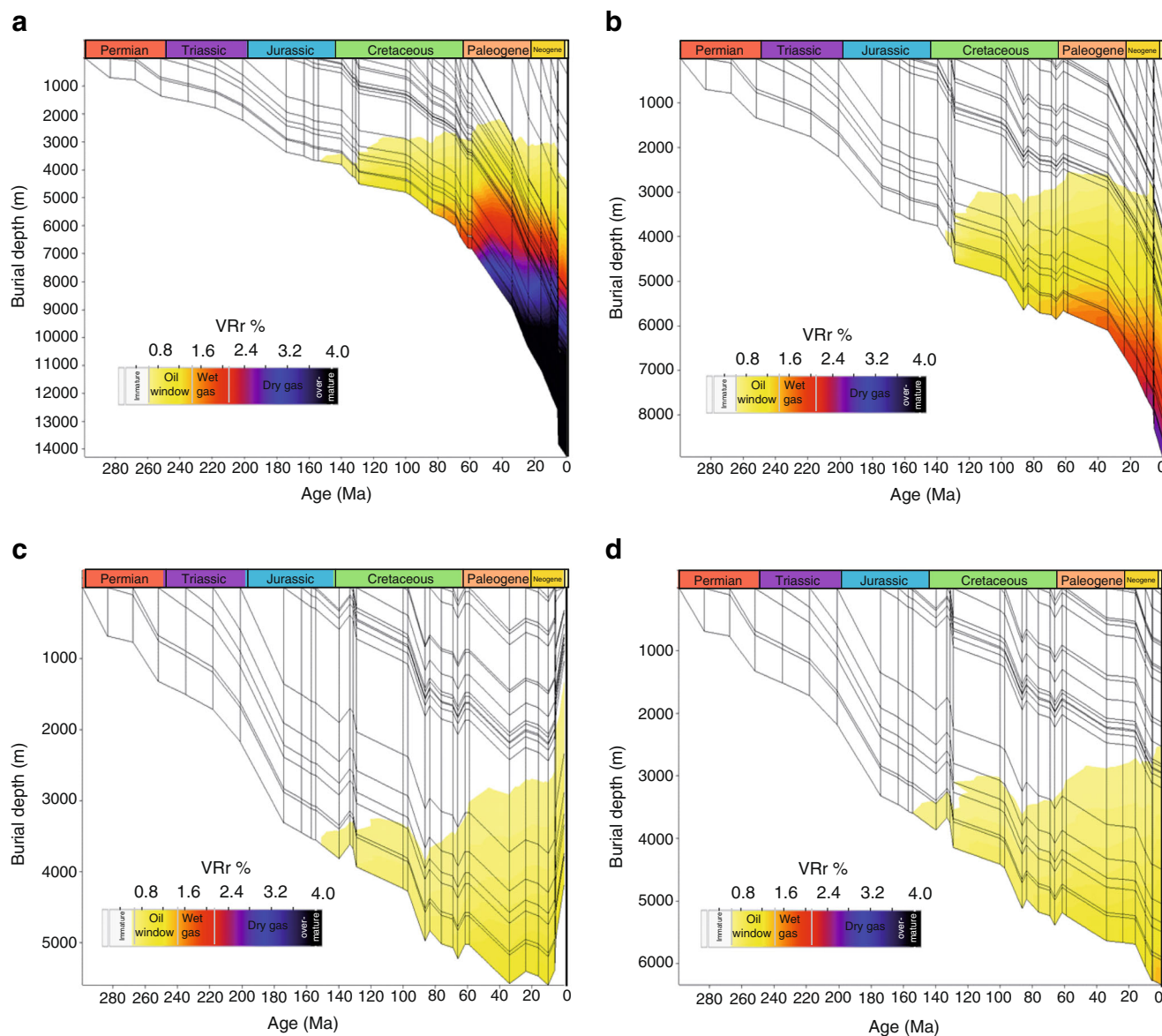


Fig. 7 a Extracted burial history and calculated vitrinite reflectance from a the deepest offshore, b margin, c uplifted mount Lebanon, and d Bekaa Valley

early oil window, only Triassic and older rocks have reached the petroleum generation stage onshore, while the younger rocks are still immature.

The effect of the thick Cenozoic cover in the Levant basin on the thermal maturity of potential source rocks can be clearly seen in maturity maps of calculated vitrinite reflectance (Fig. 8). Permian and Triassic source rocks seem to have entered the oil window everywhere in the study area during the Late Cretaceous (Fig. 8a). The Permian and Triassic source rocks experienced deep burial and maturation reaching the wet gas window in most of the offshore basin during the mid to late Eocene and the dry gas window during the

Oligo-Miocene. Since the late Miocene, the Permian and Triassic source rocks entered the overmature stage in most of the offshore Levant Basin (Fig. 8a). The maturity of Permian and Triassic source rocks decreases gradually along the margin towards the onshore where it has remained within the oil window throughout the Cenozoic, with the exception of some local deeper burial (e.g. in the Bekaa Valley) where the Permian source rocks have reached the wet gas window.

Upper Jurassic to Lower Cretaceous source rocks entered the oil window in most of the offshore basin during the mid to late Eocene, the wet gas window during

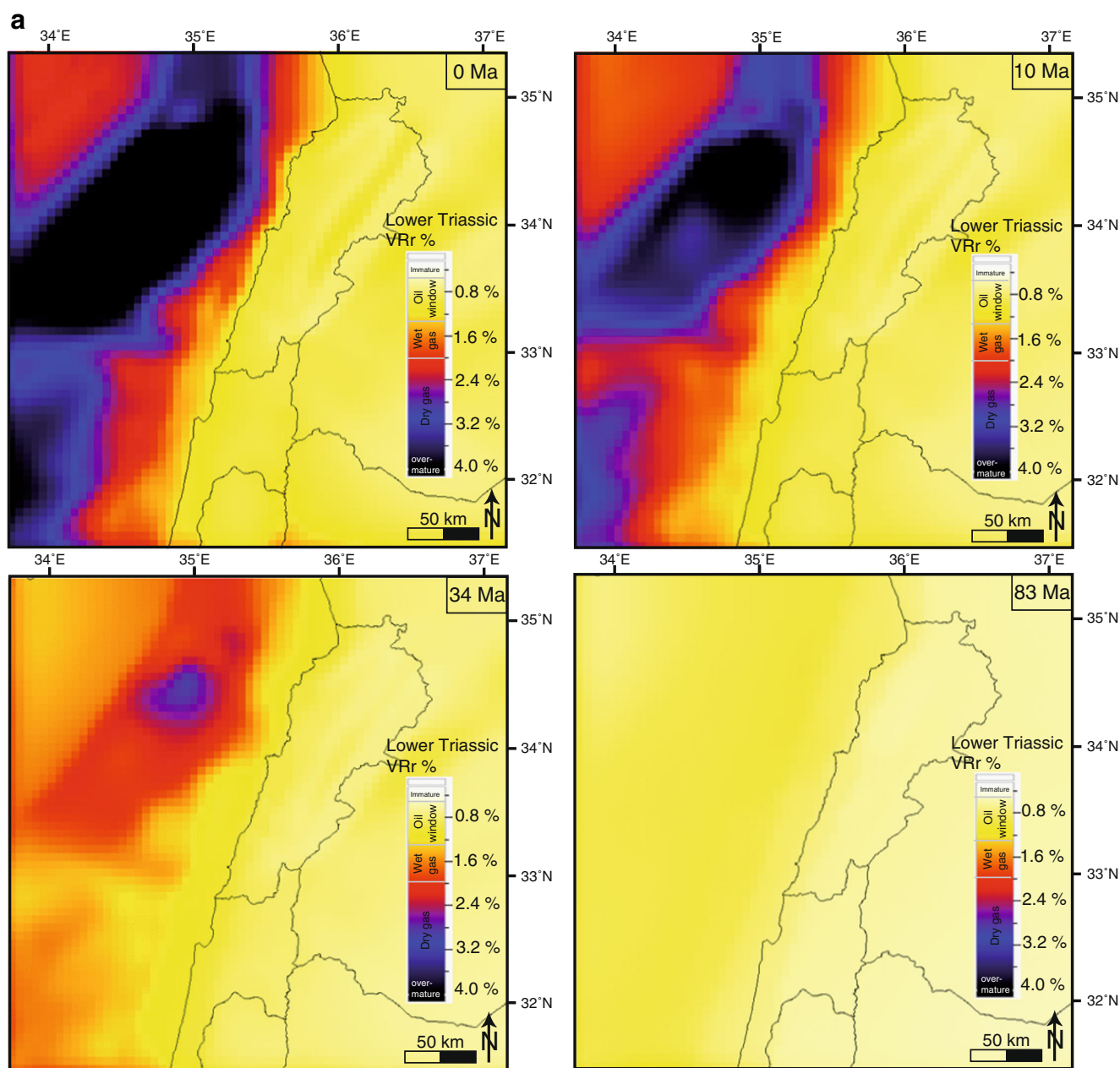


Fig. 8 Calculated vitrinite reflectance map for **a** Lower Triassic, **b** Kimmeridgian, **c** Cenomanian, and **d** Campanian. **e, f** Cross sections AA' and BB', respectively, showing calculated vitrinite reflectance at the present day (see Fig. 1 for location)

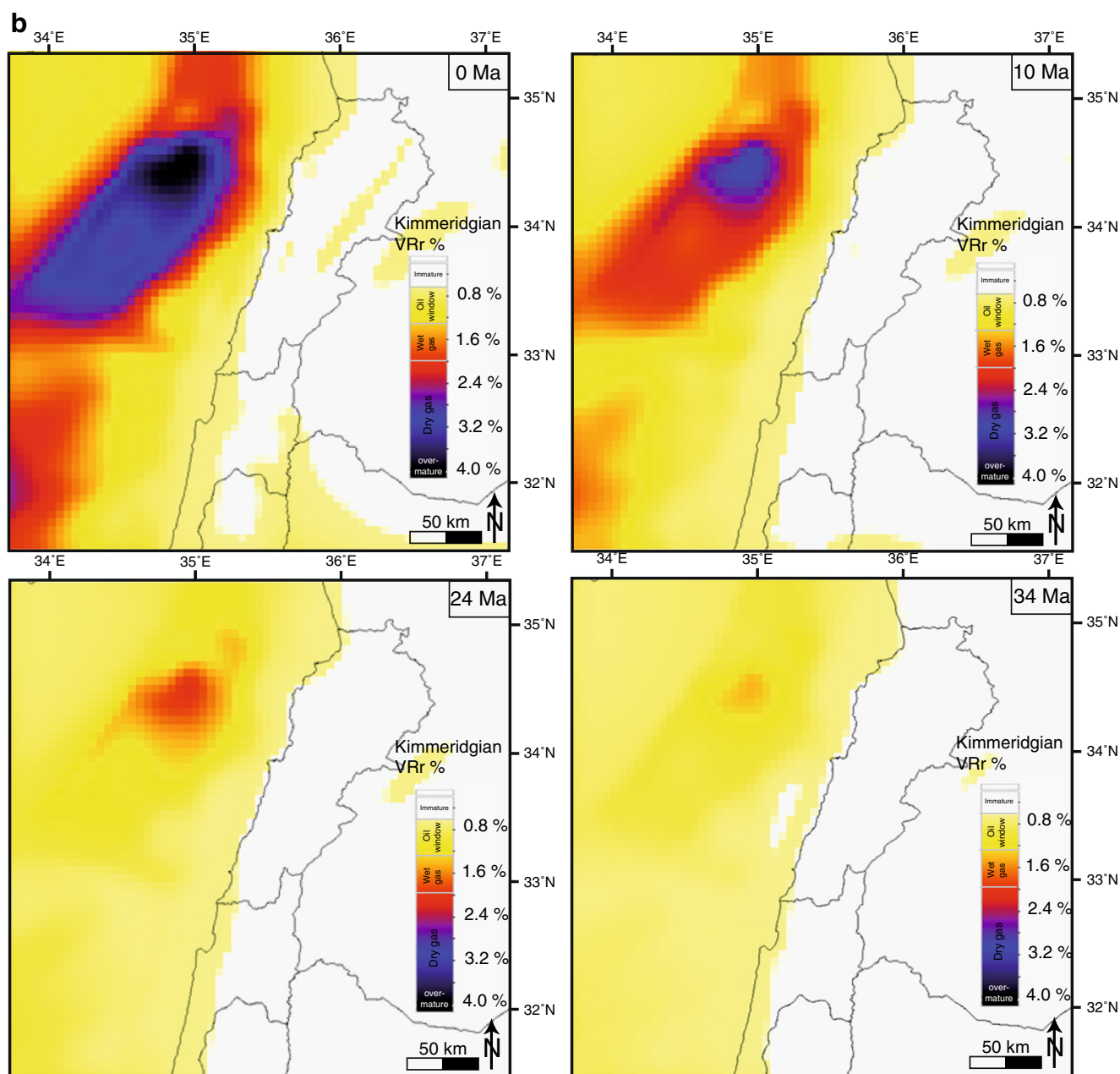


Fig. 8 (continued).

the late Miocene, and the dry gas stage at the present day (Fig. 8b). Only in the deepest part of the offshore basin are the Upper Jurassic and Lower Cretaceous source rocks overmature (Fig. 8b). Along the margin, these source rocks vary from early oil window to late oil window, while in the onshore, they remain immature or in the very early oil window with slightly higher maturities in the Bekaa Valley. The Upper Cretaceous Cenomanian source rocks entered the oil window during the late Eocene, the wet gas window in the northern offshore basin during the mid to late Miocene, and the dry gas stage at the present day (Fig. 8c). Along the

margin, the Cenomanian source rocks are at the present day in the early oil window (Fig. 8c). The Campanian and Paleocene source rocks have entered the oil window in the offshore basin during the late Oligocene (Fig. 8d). In the northern segment of the offshore Levant Basin, the Campanian and Paleocene source rocks reached the wet gas window during the late Miocene while they remained in the oil window in the rest of the offshore basin. Campanian source rocks have reached the dry gas window in the deepest part of the basin offshore Lebanon (Fig. 8d). Along parts of the margin, both source rocks have just entered the oil

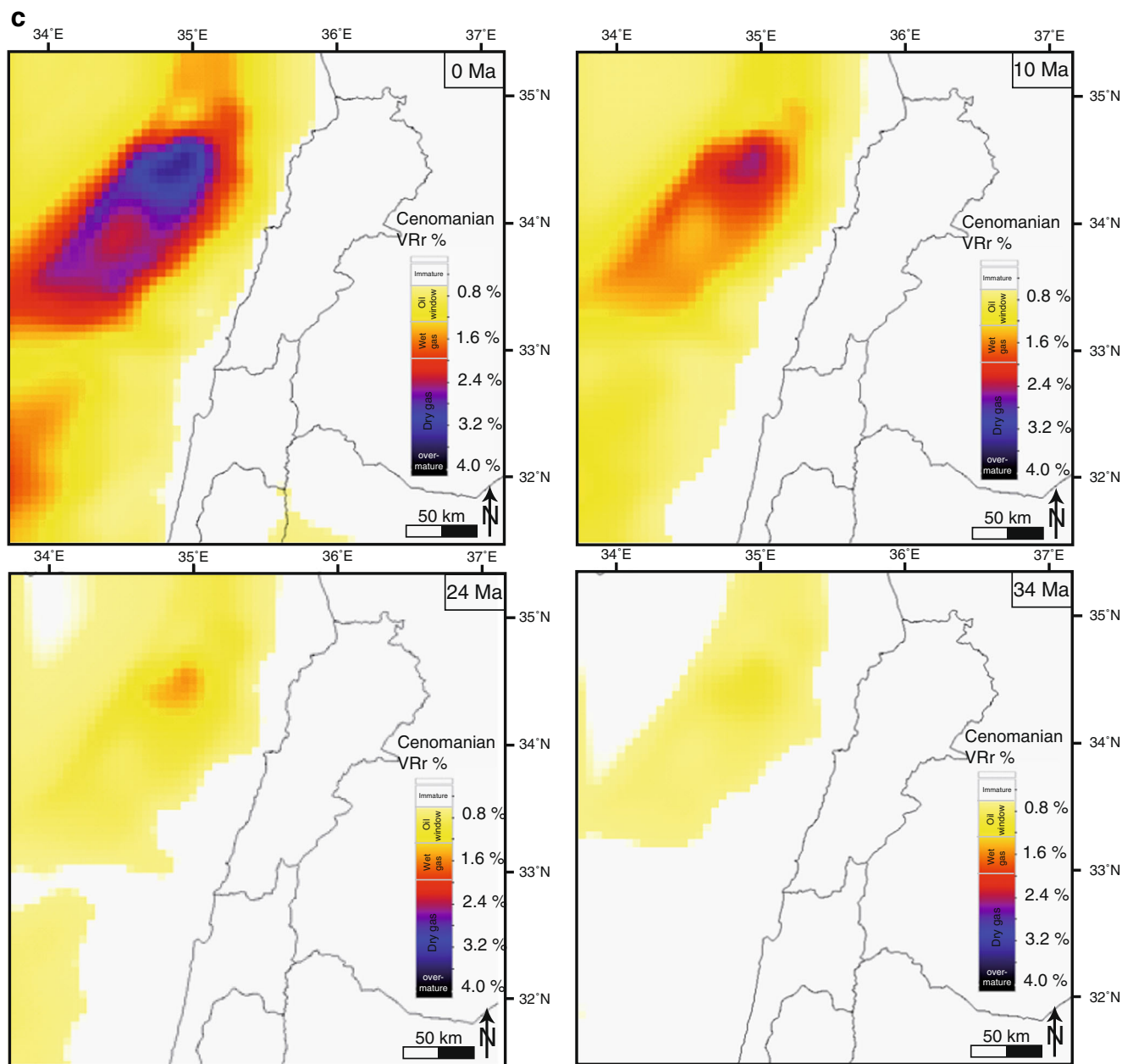


Fig. 8 (continued).

window, while in the onshore they are still immature. Figures 8e, f shows two E–W and NNE–SSW cross sections, respectively, with calculated vitrinite reflectance that reflect the very different maturation trends along the onshore and offshore.

It should be noted that the maturity stages mentioned in this chapter are standard translations of calculated vitrinite reflectance into petroleum generation stages and do not consider the different kerogen types. Therefore, type IIS bearing source rocks in the onshore area might have generated some oil although they are classified here as thermally immature.

Transformation ratio

The very different source rock maturation trends in the Levant basin, margin, and onshore imply very different potential petroleum systems in each of these realms due to different timing and depth of hydrocarbon generation. In order to assess the petroleum generation timing of a certain source rock calculated, vitrinite reflectance alone is not sufficient, but transformation ratios are also needed.

Transformation ratio maps (Fig. 9) have been extracted for several potential source rocks. The Upper Jurassic Kimmeridgian source rocks started generating hydrocarbons

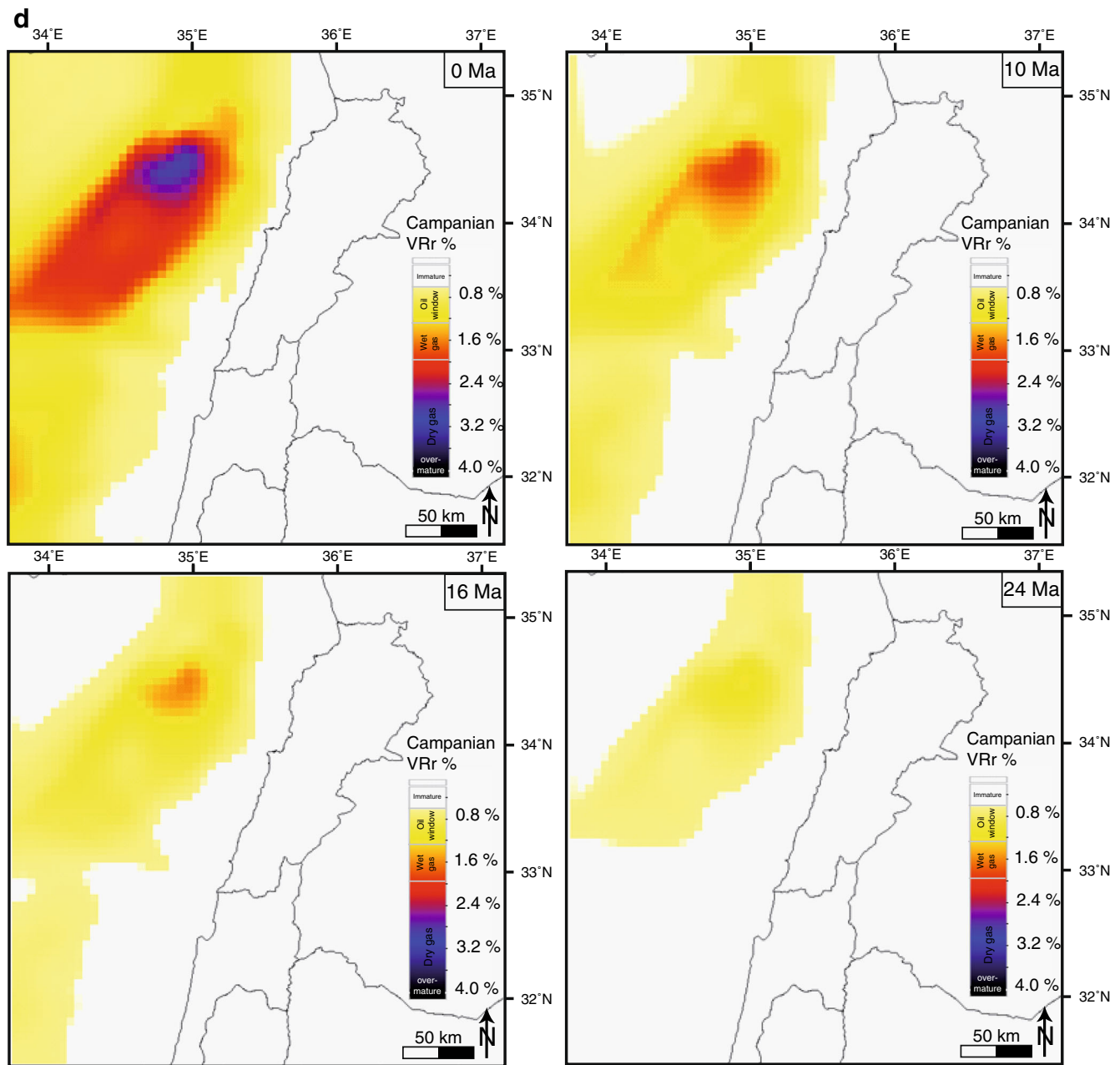


Fig. 8 (continued).

in most of the offshore basin during the very Late Cretaceous and early Paleocene, and have reached 100 % transformation ratio by the late Miocene (Fig. 9a). Along the margin, hydrocarbon generation from the Kimmeridgian source rock continues to the present day (Fig. 9a). The Lower Cretaceous Neocomian source rocks show a similar trend, with a slightly younger onset of hydrocarbon generation (Fig. 9b). In the onshore, limited hydrocarbon generation have occurred from the Kimmeridgian source rocks in some of the coastal areas and inland topographic lows since the late Miocene (Fig. 9a),

while the Neocomian source rocks did not generate any hydrocarbons onshore (Fig. 9b). The generated Kimmeridgian hydrocarbons onshore have most probably been washed by meteoric water which have been invading the Jurassic and the overlying rock succession since the emergence of Mount Lebanon in the late Cenozoic (Nader and Swennen 2004).

Campanian and Paleocene source rocks have very similar hydrocarbon generation histories starting in the late Oligocene in the deepest part of the offshore basin and remaining restricted to the offshore basin while almost no hydrocarbon genera-

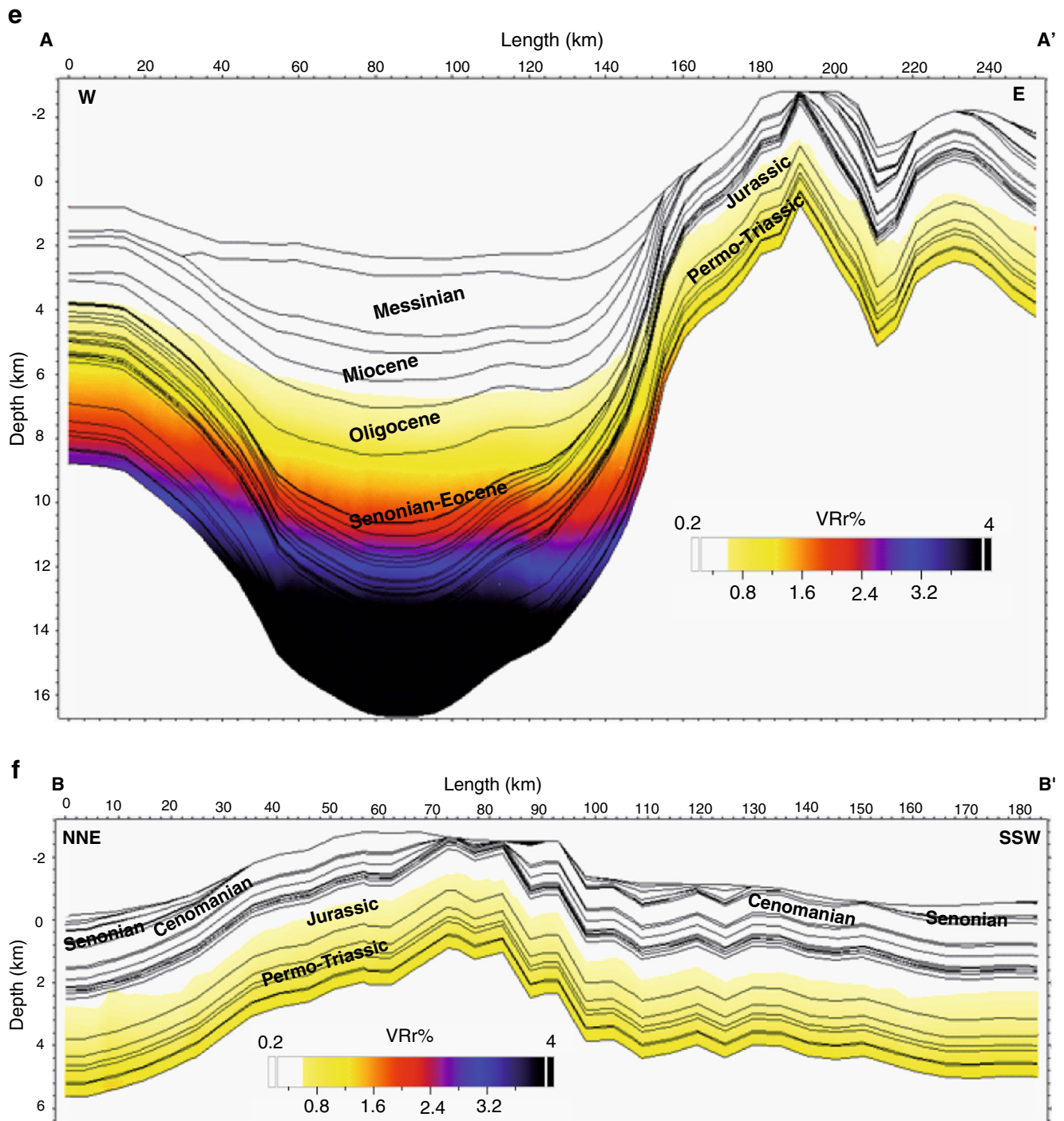


Fig. 8 (continued).

tion have occurred from those source rocks along the margin or in the onshore (Fig. 9c, d). The transformation ratio maps of the Campanian source rock were calculated using the kinetics of type II kerogen (Campanian 1) (Fig. 5b). Another simulation was run using the kinetics of type IIS kerogen (Campanian 2) (Fig. 5c) which resulted in a much earlier onset

of hydrocarbon generation from Campanian source rocks in the offshore Levant Basin and considerable generation along the margin, while in the onshore, only minor hydrocarbon generation occurred in the Bekaa Valley. Based on the conceptual depositional model proposed by Bou Daher et al. (2015), suggesting that type II kerogen with high activation

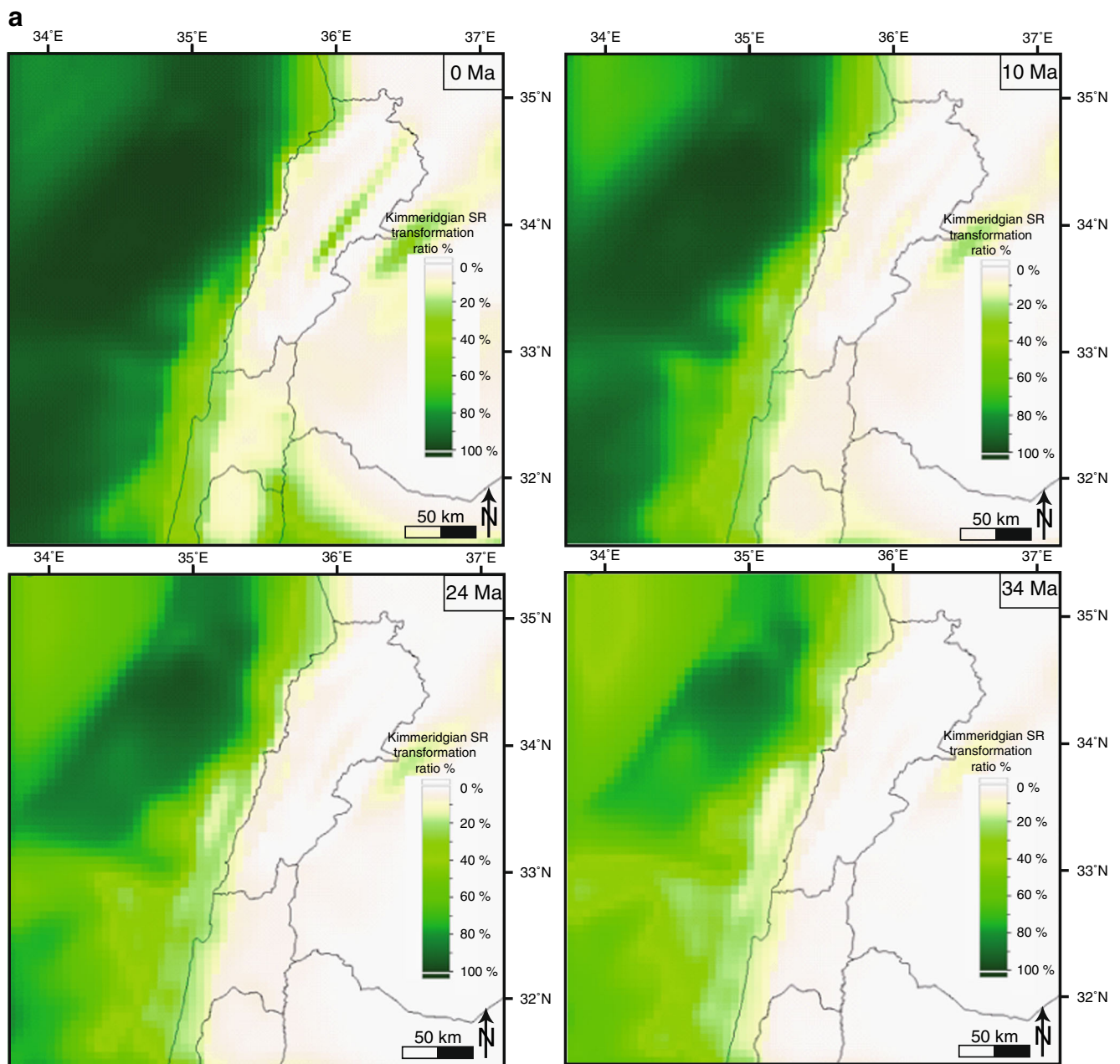


Fig. 9 Source rock transformation ratio maps for **a** Kimmeridgian, **b** Lower Cretaceous (Neocomian), **c** Campanian, and **d** Paleocene

energies would be expected for the Campanian source rocks in the basin and margin, while along most of the onshore type IIS kerogen with lower activation energies is more representative, we suggest that the scenario reported in Fig. 9c is to our best knowledge the representative case for the Levant Basin and margin. The second scenario, however, is validated for the onshore realm through the presence of large amounts of immature solid bitumen south of the Bekaa Valley which is typical for early stages of hydrocarbon generation from type IIS kerogen (Bou Daher et al. 2015).

Petroleum systems

The results presented and discussed above illustrate the quality and quantity of known source rocks and the timing of hydrocarbon generation from key source rock intervals in different realms of the study area and indicate that different potential source rocks can be active at different times in the offshore, margin, and onshore. However, for a successful petroleum system to be present, several other factors need to come in place. These include migration paths, reservoir

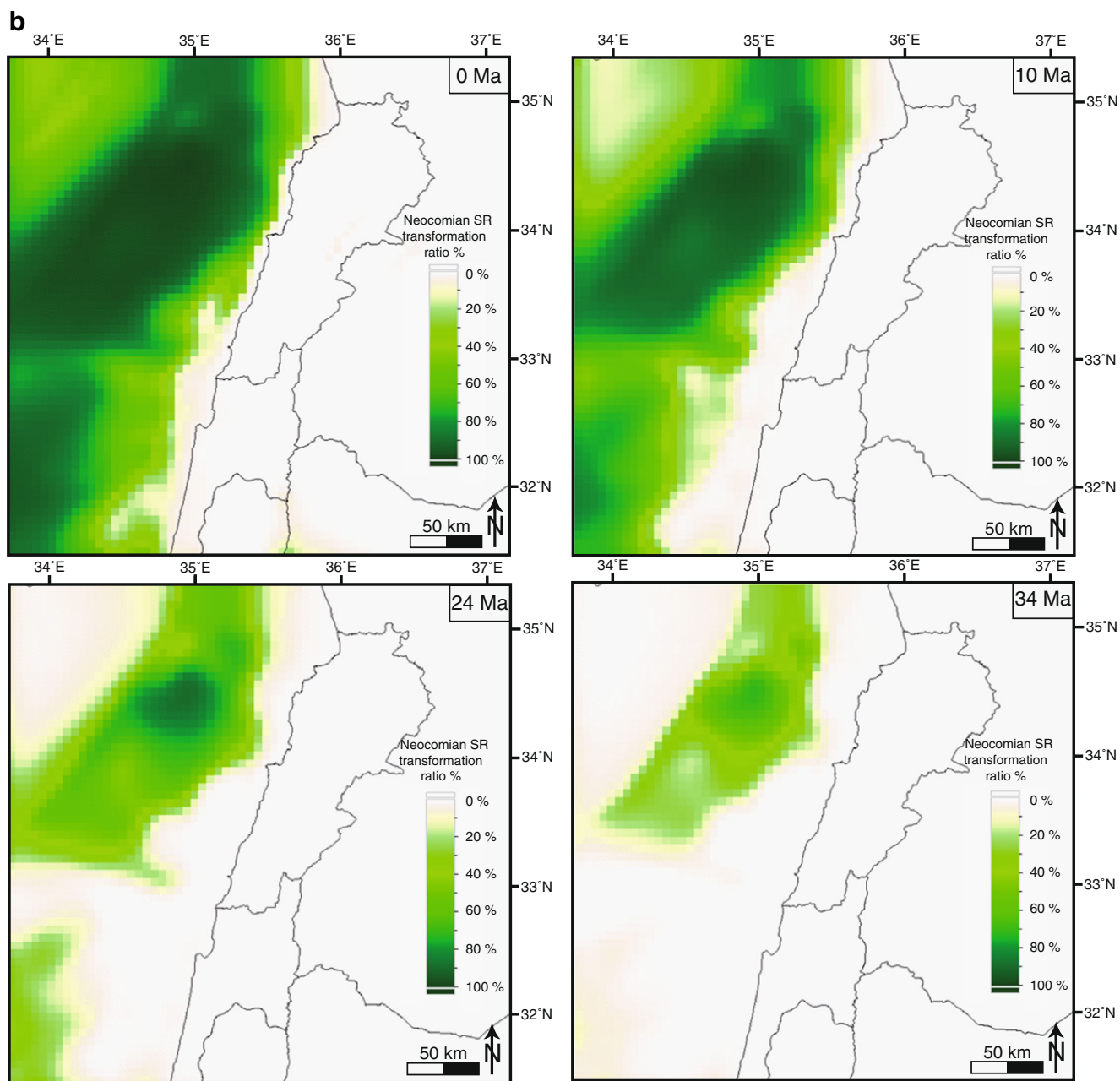


Fig. 9 (continued).

quality, trapping, sealing, and seal integrity. In the Permian–Triassic succession, rock units with source, reservoir, and seal potential have been reported in Israel (Gardosh et al. 2008) and in Syria (Brew et al. 2001; Lučić et al. 2010). Triassic source rocks have been proved to charge Middle Triassic, Middle Jurassic, and Upper Cretaceous reservoirs in Syria (Abboud et al. 2005). In the deepest part of the offshore Levant Basin, hydrocarbon generation from Permian–Triassic source rocks occurs between 90 and 34 Ma and petroleum can accumulate in tilted rift blocks (Fig. 10). Along

the margin, hydrocarbon generation from the Permian to Triassic starts at later stages (75 Ma) and continues in the onshore till the present day. Onshore structures, such as the Qartaba box fold (Nader 2014), can be an excellent trap for Permian–Triassic hydrocarbons sealed by the Upper Triassic anhydrites that are expected to be present in Lebanon, as an extension of the Kurrachine anhydrites of the Palmyra Basin. Such evaporite deposits could protect the Permian–Triassic succession in Lebanon from water washing and karstification that seems to have affected the Jurassic and younger rock units

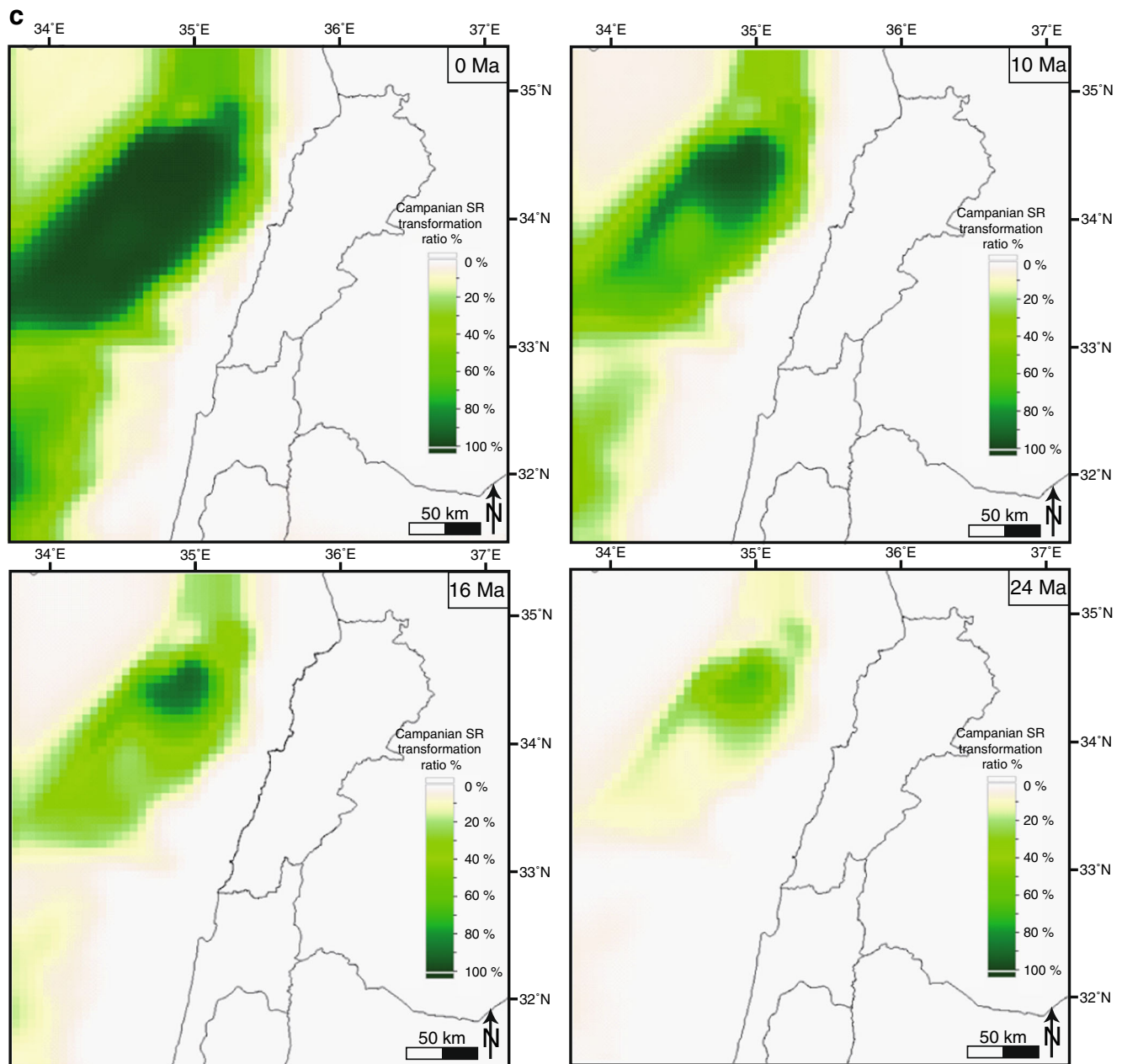


Fig. 9 (continued).

(Renouard 1955; Beydoun 1977; Beydoun and Habib 1995; Brew et al. 2001; Lučić et al. 2010). Hydrocarbons from Jurassic and Lower Cretaceous source rocks were generated in the deepest basin between 75 and 24 Ma and might have accumulated in reactivated Mesozoic structures along the margin (Fig. 10) (Ghalayini et al. 2014). Jurassic and Lower Cretaceous rocks exposed onshore have excellent reservoir potential (Nader 2014) and can be sealed by the Upper Jurassic (Kimmeridgian) shales, marls, and volcanics and the

Lower Cretaceous (Albian) marls, respectively (Nader 2014). Oil has been reported in Lower Cretaceous sandstones in the Mango field offshore Sinai and in the Euphrates Graben (OAPEC Annual Report 2002; Gardosh et al. 2008; Nader 2014). Oil and gas shows have been also reported from Middle Jurassic limestones Yam-2 and Yam Yafi-1 wells off the coast of Israel (Gardosh et al. 2008). One very promising structure that can trap Jurassic and Lower Cretaceous hydrocarbons is the box fold Ile du Palmier off the coast of Tripoli

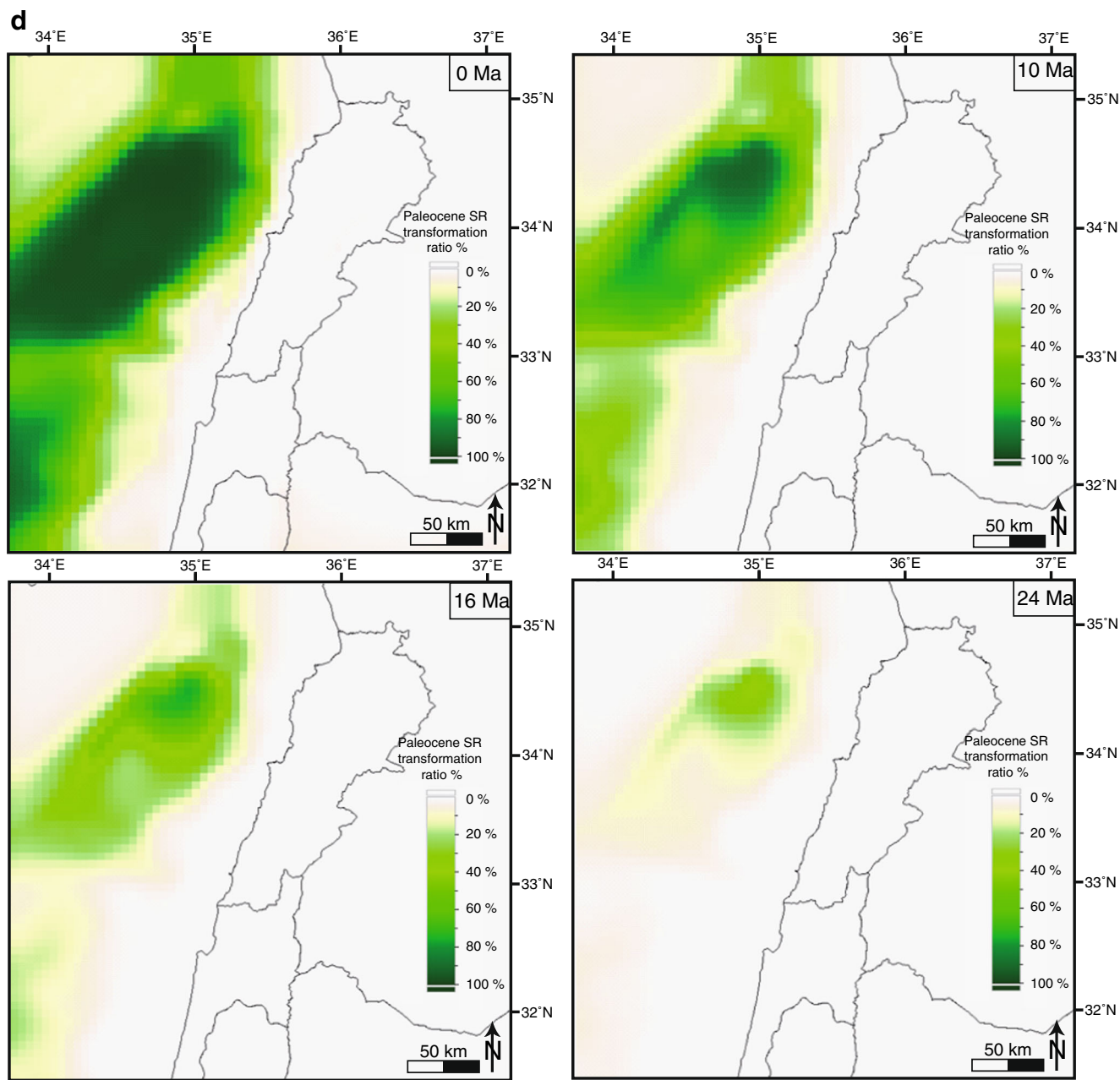


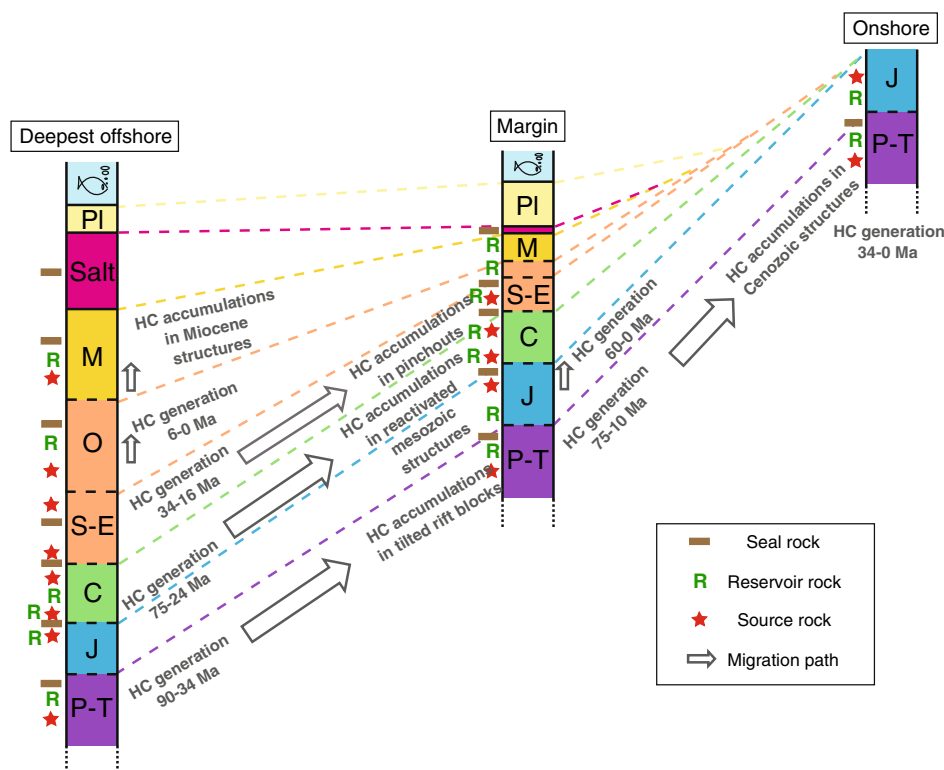
Fig. 9 (continued).

(Fig. 1). The Jurassic and Lower Cretaceous reservoirs in this structure would be protected from water washing by the distance from the uplifted intake area (Beydoun 1977; Nader and Swennen 2004).

Upper Cretaceous source rocks are only mature in the deep basin, and in the deepest part of the basin they produced hydrocarbons between 34 and 16 Ma. Upward vertical migration from Upper Cretaceous (particularly Campanian) source rocks in the offshore basin would be impeded by the presence of a

very good Paleocene seal. Thus, migration would most probably occur laterally into marginal pinchouts and reactivated Mesozoic structural traps (Fig. 10). Lower Maastrichtian calcareous turbidites were reported along the coast in Northern Lebanon (Hawie et al. 2013b). These can be potential reservoirs for Upper Cretaceous hydrocarbons, sealed by the Paleocene marls. Paleocene and Eocene source rocks produce hydrocarbons at slightly younger ages and might be charging Oligocene and Miocene reservoirs in offshore structures.

Fig. 10 Schematic diagram summarizing the potential petroleum systems of the Levant basin offshore, margin, and onshore Lebanon



Oligocene potential source rocks are in the oil window at the present day and have started to generate hydrocarbons at around 6 Ma and thus can charge Oligocene and Miocene reservoirs in young structures (Fig. 10), such as the NNE–SSW trending anticlines affecting the Oligocene–Miocene succession in the offshore basin (Ghalayini et al. 2014). Disseminated terrestrial organic matter in the upper Oligocene has been proved to be an important source rock offshore the Nile Delta (Villinski 2013).

Sensitivity and uncertainty

The thermal history of a sedimentary basin is controlled by many parameters, most of which are often very poorly constrained, particularly in frontier basins such as the Levant Basin. Testing the sensitivity of the system to some of those parameters can help in quantifying the effects they have on the temperature of the basin and thus on source rocks maturation. In this study, we have extracted a 1D model from the deepest part of the offshore basin and tested for the sensitivity of the present-day geothermal gradient to lithologies' variation, crustal thickness, and depth of the lithospheric–asthenospheric boundary (LAB). The pre-Messinian Cenozoic lithology was varied from carbonate dominated (low radiogenic heat production, high thermal conductivity) to siliciclastic dominated

(high radiogenic heat production, low thermal conductivity). The resulting difference in the present-day geothermal gradient between the tested scenarios affects the pre-Miocene succession shifting the temperatures by up to 18 °C (Fig. 11a). This temperature variation seems to have no effect on the Miocene succession, most probably due to the chimney effect exerted by the high thermal conductivity of the thick Messinian salt (Fig. 11a).

The present-day crustal thickness was varied from 8 to 20 km (Netzeband et al. 2006). The resulting effect on the present-day geothermal gradient increases with depth, reaching a difference of 28 °C between end member scenarios for the deepest intervals (Fig. 11b). The effect of crustal thickness is minor for shallow intervals (Fig. 11b).

The depth of the LAB was varied from 80 to 120 km (Jiménez-Munt et al. 2006; Segev et al. 2006) which had a major effect on the present-day geothermal gradient (Fig. 11c). The effect of these three modified parameters on source rock maturation and petroleum systems is summarized in Fig. 12, showing a significant impact on the expected depth of the oil and the gas windows. The thickness of the pre-Messinian biogenic zone also varies between 700 and 1500 m, indicating that under any scenario, the pre-salt Miocene in the deep offshore basin would have a biogenic gas potential in a zone of at least 700 m, assuming a biogenic zone from 0 to 80 °C (Fig. 12).

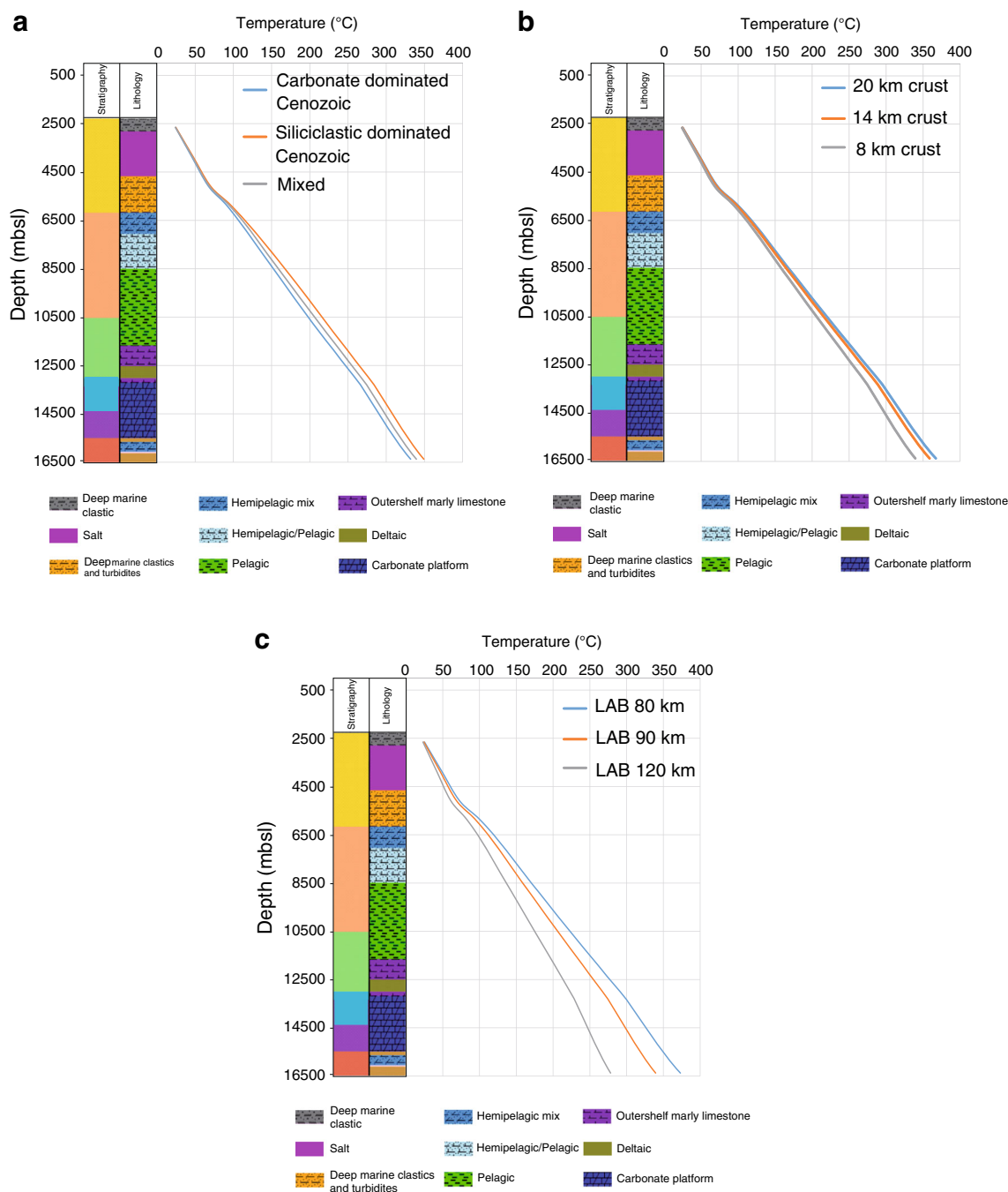


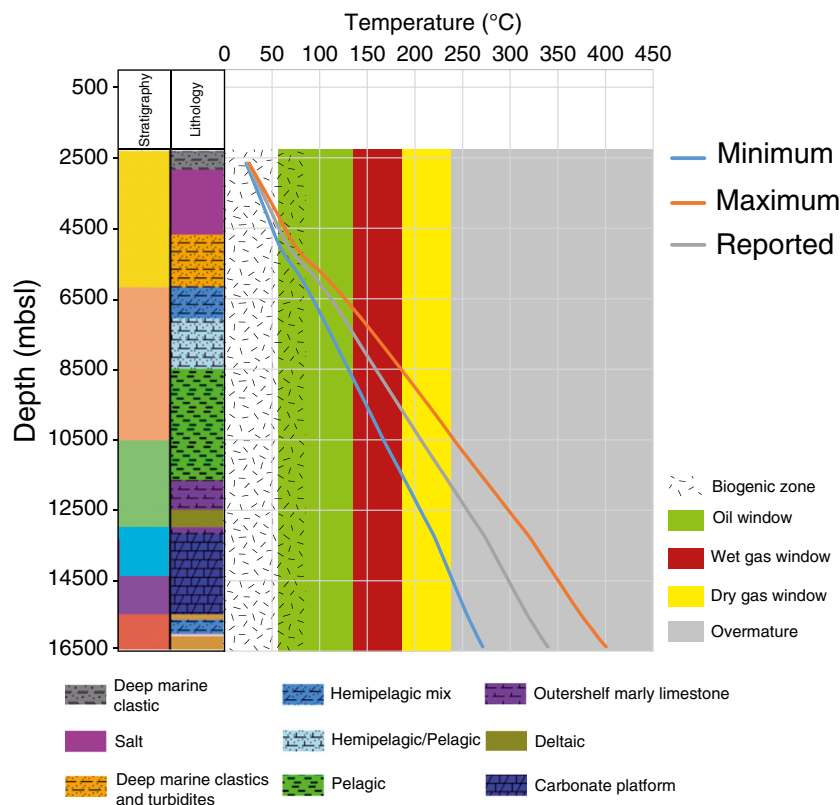
Fig. 11 Extracted 1D model from the deepest offshore basin showing the sensitivity of the system to changes in **a** lithology, **b** crustal thickness, and **c** depth of the LAB. See Fig. 1 for location. Colour-coded stratigraphy

based on international chronostratigraphic chart. Note that the first 2300 m depth are water column

In an underexplored basin such as the Levant Basin, uncertainties related to hydrocarbon generation timing can raise not only from uncertainty in thermal history but also from several other parameters. TOC values, source rock presence, quality and thickness, hydrocarbon generation kinetics, and lateral changes in organofacies are parameters that have an important impact on hydrocarbon generation and eventually on

petroleum systems. Further uncertainties that should be considered when assessing potential petroleum systems in the Levant Basin, particularly offshore, are related to reservoir quality, migration paths, and seal integrity. A catastrophic event that had an enormous impact on seal integrity and petroleum systems is the Messinian salinity crisis. The fast drop of sea level by around 2000 m resulted in a drop in pressure,

Fig. 12 Extracted 1D model from the deepest offshore basin showing the minimum and the maximum geothermal gradients and their effect on maturity and petroleum systems. See Fig. 1 for location. Colour-coded stratigraphy based on international chronostratigraphic chart. Note that the first 2300 m depth are water column



an increase in temperature, and fast salt deposition. The surface temperature change during the Messinian is minor and has little effect on the petroleum systems. The hydrostatic pressure drop, however, would result in higher pore pressure and possible seal fracturing within the shallow biogenic system (Wygrala et al. 2014). The effects of this event are thought to attenuate in deeper biogenic systems (e.g. Tamar, Leviathan, Aphrodite) and in speculative thermogenic systems.

Conclusions

The results presented in this study proved the presence of several potential petroleum source rocks along the eastern margin of the Levant Basin and suggest different prospective working petroleum systems in the offshore, margin, and on-shore Lebanon.

An Upper Cretaceous–Oligo-Miocene mixed thermogenic and biogenic system is expected in the offshore. In the pre-Messinian salt succession, the thickness of the biogenic zone can vary between 700 and 1500 m throughout the offshore basin, rendering the NNE–SSW offshore anticlines which affect the Oligo-Miocene succession an excellent target for biogenic and thermogenic hydrocarbons. The biogenic hydrocarbon potential decreases towards the margin and onshore due to the lack of appropriate seal.

A Jurassic–Lower Cretaceous petroleum system is expected along the margin, where Lower Cretaceous sandstones and Upper Jurassic Carbonates, which have excellent reservoir quality in the onshore, could be charged with oil and gas from Jurassic and Lower Cretaceous shales.

A Permo-Triassic petroleum system is expected in the onshore, where Lower Triassic reservoirs sealed by Upper Triassic evaporites in Miocene structures would be filled with gas from Triassic (and possibly deeper) source rocks.

Kinetic results derived from Campanian source rocks showed a variation of bulk hydrocarbon generation kinetics attributed to lateral variation of organofacies within the same source rock. These lateral source rock quality changes have an important impact on the assessment of hydrocarbon generation particularly in a frontier basin. Thus, a detailed understanding of a source rock's depositional environment at the sampling sites is essential for a better source rock extrapolation at a basin scale.

Acknowledgments The authors would like to thank the DAAD (German Academic Exchange Service) for the financial support, the Lebanese Ministry of Energy and Water (Petroleum Administration) for providing data and field access, as well as the BeicipFranlab for providing us with a *TemisFlow*TM license. Thanks to Bernard Carpentier, Isabelle Kowalewski, and Eric Kohler for their invaluable assistance and discussions. Thanks to Julien Labaume, Daniel Pillot, G eremie Letort, Said Youssouf, Ramon Martinez, and Herman Ravelojaona for the analytical work and the timely delivery of results.

References

- Abboud M, Philip RP, Allen J (2005) Geochemical correlation of oils and source rocks from central and NE Syria. *J Pet Geol* 28:203–218
- Abdel-Rahman A-FM, NASSAR P (2004) Cenozoic volcanism in the Middle East: petrogenesis of alkali basalts from northern Lebanon. *Geol Mag* 141(5):545–563
- Adiyaman Ö, Chorowicz J (2002) Late Cenozoic tectonics and volcanism in the northwestern corner of the Arabian plate: a consequence of the strike-slip Dead Sea fault zone and the lateral escape of Anatolia. *J Volcanol Geotherm Res* 117:327–345
- Ayres MG, Bilal M, Jones MV, Slentz LW, Tartir M, Wilson AO (1982) Hydrocarbon habitat in main producing areas, Saudi Arabia. *AAPG Bull* 66:1–19
- Bar, O., Gvirtsman, Z., Feinstein, S., Zilberman, E., 2011. Late Tertiary subsidence of the Levant margin: distinction between sedimentary load and tectonics. *Geological Survey of Israel* 20/2011, pp. 33
- Behar F, Lorant F, Lewan MD (2008) Role of NSO compounds during primary cracking of a type II kerogen and a type III lignite. *Org Geochem* 39:1–22
- Beydoun ZR (1977) Petroleum prospects of Lebanon: re-evaluation. *AAPG Bull* 61:43–64
- Beydoun, Z. R., 1999. Evolution and development of the Levant (Dead Sea Rift) transform system: a historical-chronological review of a structural controversy. In: Mac Niocail, C., Ryan, P.D. (Eds.), *Continental tectonics*, Geological Society, London, Special Publications. 164, 239–255
- Beydoun ZR, Habib JG (1995) Lebanon revisited: new insights into Triassic hydrocarbon prospects. *J Petrol Geol* 18(1):75–90
- Bou Dagher-Fadel M, Clark G-N (2006) Stratigraphy, paleoenvironment and paleogeography of Maritime Lebanon: a key to Eastern Mediterranean Cenozoic history. *Stratigraphy* 3:81–118
- Bou Daher S, Nader FH, Strauss H, Littke R (2014) Depositional environment and source-rock characterisation of organic-matter rich Upper Turonian/Upper Campanian carbonates, Northern Lebanon. *J Pet Geol* 37:1–20
- Bou Daher S, Nader FH, Müller C, Littke R (2015) Geochemical and petrographic characterization of Campanian-Lower Maastrichtian calcareous petroleum source rocks of Hasbayya, South Lebanon. *Mar Pet Geol* 64:304–323
- Bowman SA (2011) Regional seismic interpretation of the hydrocarbon prospectivity of offshore Syria. *GeoArabia* 16:95–124
- Brew G, Barazangi M, Al-Maleh AK, Sawaf T (2001) Tectonic and geologic evolution of Syria. *GeoArabia* 6(4):573–615
- Chaimov T, Barazangi M, Al-Saad D, Sawaf T, Gebran A (1992) Mesozoic and Cenozoic deformation inferred from seismic stratigraphy in the southwestern intracontinental Palmyride fold-thrust belt. *Syria Bull Geol Soc Am* 104:704–715
- Dubertret, L., 1955. Carte géologique du Liban au 1/200000 avec notice explicative. République Libanaise, Ministère des Travaux Publiques, Beirut, p. 74
- Dubertret L (1975) Introduction à la carte géologique au 1/50000 du Liban. *Notes et Mémoires sur le Moyen-Orient* 23:345–403
- Dubille, M., Thomas D., 2012. Petroleum system assessment of the offshore Lebanon Thorough 3D basin modeling. Presentation, Lebanese International Petroleum Exploration Forum (LIPE), Beirut, Lebanon
- Durand B, Nicaise G (1980) Procedure of kerogen isolation. In: Durand B (ed) *Kerogen, insoluble organic matter from sedimentary rocks*. Editions Technip, Paris, pp. 13–34
- Eckstein Y, Simmons G (1978) Measurement and interpretation of terrestrial heat flow from Israel. *Geothermics* 6:117–142
- Esestine P, Hewitt A, Hodgson N (2016) Zohr—a newborn carbonate play in the Levantine Basin, East-Mediterranean. *First Break* 34:87–93
- Feinstein S, Aizenshtat Z, Miloslavsky I, Gerli NP, Slager J, McQuilken J (2002) Genetic characterization of gas shows in the east Mediterranean offshore of southwestern Israel. *Organic Geochem* 33(12):1401–1413
- Feinstein, S., Aizenshtat, Z., Miloslavsky, I., Goldberg, M., Obermagher, M., 2013. Oil groups in the East Mediterranean continental margin and onshore, Israel. AAPG Search and Discovery Article #90161©2013 AAPG European Regional Conference, Barcelona, Spain, 8–10 April 2013
- Gardosh, M., 2013. Exploration in the Eastern Mediterranean, Offshore Israel—Ongoing Success and Future Challenges AAPG Search and Discovery Article #90161©2013 AAPG European Regional Conference, Barcelona, Spain, 8–10 April 2013
- Gardosh, M., Druckman, Y., Buchbinder, B., Rybakov, M., 2008. The Levant Basin Offshore Israel: stratigraphy, structure, tectonic evolution and implications for hydrocarbon exploration. *Geophysical Institute of Israel*. 429/328/08, pp. 119
- Gardosh, M. A., Garfunkel, Z., Druckman, Y., Buchbinder, B., 2010. Tethyan rifting in the Levant region and its role in Early Mesozoic crustal evolution. In: Homberg C. and Bachmann M. (Eds), *Evolution of the Levant Margin and Western Arabia Platform since the Mesozoic*. *Geol. Soc. Lond., Spec. Publ.*, 341, 9–36
- Garfunkel Z (1989) Tectonic setting of Phanerozoic magmatism in Israel. *Israel J Earth-Sci* 38:51–74
- Garfunkel Z (1992) Darfur-Levant array of volcanics—a 140-Ma-long record of hot spot beneath the African-Arabian continent and its bearing on Africa's absolute motion. *Israel J Earth Sci* 40:135–150
- Garfunkel Z (1998) Constrains on the origin and history of the Eastern Mediterranean basin; collision-related processes in the Mediterranean region. *Tectonophysics* 298:5–35
- Ghalayini R, Daniel J-M, Homberg C, Nader FH, Comstock JE (2014) Impact of Cenozoic strike-slip tectonics on the evolution of the northern Levant Basin (offshore Lebanon). *Tectonics* 33. doi:10.1002/2014TC003574
- Gomez F, Khawlie M, Tabet C, Darkal AN, Khair K, Barazangi M (2006) Late Cenozoic uplift along the northern Dead Sea transform in Lebanon and Syria. *Earth Planet Sci Lett* 241:913–931
- Hardenberg MF, Robertson AHF (2007) Sedimentology of the NW margin of the Arabian plate and the SWNE trending Nahr el Kabir half graben in northern Syria during the latest Cretaceous and Cenozoic. *Sediment Geol* 201:231–266
- Hawie, N 2014. Architecture, geodynamic evolution and sedimentary filling of the Levant Basin: a 3D quantitative approach based on seismic data. PhD thesis, Université Pierre et Marie Curie. pp. 250
- Hawie N, Gorini C, Deschamps R, Nader FH, Montadert L, Grajeon D, Baudin F (2013a) Tectono-stratigraphic evolution of the northern Levant Basin (offshore Lebanon). *Mar. Pet Geol* 48:392–410
- Hawie N, Deschamps R, Nader FH, Gorini C, Müller C, Desmares D, Hoteit A, Granjeon D, Montadert L, Baudin F (2013b) Sedimentologic and stratigraphic evolution of northern Lebanon since the late Cretaceous: implications on the Levant margin and basin. *Arab J Geosci*. doi:10.1007/s12517-013-0914-5
- Jiménez-Munt I, Sabadini R, Gardi A, Bianco G (2006) Active deformation in the Mediterranean from Gibraltar to Anatolia inferred from numerical modeling and geodetic and seismological data. *J Geophys Res* 108(B1):2003. doi:10.1029/2001JB001544
- Khair K, Khawlie M, Haddad F, Barazangi M, Chaimov T, Seber D (1993) Gravity modeling and geologic setting and tectonics of the central segment of the Dead Sea fault zone. *Geology* 21:739–742
- Khair K, Tsokas GN, Sawaf T (1997) Crustal structure of the northern Levant region: multiple source Werner deconvolution estimates for Bouguer gravity anomalies. *Geophys J Int* 128:605–616
- Kolonic S, Sinninghe Damsté JS, Böttcher ME, Kuypers MMM, Kuhnt W, Beckmann B, Scheeder G, Wagner T (2002) Geochemical characterization of Cenomanian/Turonian black shales from the Tarfaya Basin (SW Morocco). *J Pet Geol* 25:325–350
- Littke R, Urai JL, Uffmann AK, Risvanis F (2012) Reflectance of dispersed vitrinite in Palaeozoic rocks with and without cleavage:

- implications for burial and thermal history modeling in the Devonian of Rursee area, northern Rhenish Massif, Germany *Int J Coal Geol* 89:41–50
- Lučić, D., Foršek, G., et al. 2003, Depositional environment and reservoir properties of Kurrachine Dolomite and Markada Formation in Central Palmyrides, Syria, Abstract, 22nd IAS Meeting of Sedimentology, Opatija, 110–111
- Lüning D, Ivković Z, Foršek G, Takač D, Bubnić J, Koch G (2010) Depositional sequences and palynology of Triassic carbonate-evaporite platform deposits in the Palmyrides, Syria in VAN BUCHEM, F. S. P., GERDES, K. D. & ESTEBAN, M. (eds) Mesozoic and Cenozoic carbonate systems of the Mediterranean and the Middle East: stratigraphic and diagenetic reference models. *Geol Soc Lond, Spec Publ* 329:43–63
- Lüning S, Kolonic S, Belhadj EM, Belhadj Z, Cota L, Baric G, Wagner T (2004) Integrated depositional model for the Cenomanian–Turonian organic-rich strata in North Africa. *Earth Sci Rev* 64:51–117
- Makris J, Stobbe C (1984) Physical properties and state of the crust and upper mantle of the Eastern Mediterranean Sea deduced from geophysical data. *Mar Geol* 55:347–363
- Makris J, Ben-Avraham Z, Behle A, Ginzburg P, Gieze P, Steinmetz L, Whitmarsh RB, Eleftheriou S (1983) Seismic refraction profiles between Cyprus and Israel and their interpretation. *Geophys J Royal Astron Soc* 75:575–591
- Montadert L, Nicolaides S, Semb PH, Lie Ø (2014) Petroleum systems offshore Cyprus. In: Marlow L, Kendall C, Yose L (eds) Petroleum Systems of the Tethyan Region, AAPG, Memoir, vol 106, pp. 301–334
- Moretti I, Kerdraon Y, Rodrigo G, Huerta F, Griso JJ, Sami M, Said M, Ali H (2010) South Alamein petroleum system (Western Desert, Egypt). *Pet Geosci* 16:121–132
- Müller, C., Higazi, F., Hamdan, W., Mroueh, M., 2010. Revised stratigraphy of the Upper Cretaceous and Cenozoic series of Lebanon based on nanofossils. In: Geological Society London Special Publication, 341, pp. 287–303
- Morris RJ (1980) Middle East; stratigraphic evolution and oil habitat. *AAPG Bull* 64:597–618
- Nader, F.H., 2003. Petrographic and geochemical study of the Kesrouane Formation (Jurassic), Mount Lebanon: implications on dolomitization and petroleum geology. Unpublished PhD thesis, Katholieke Universiteit Leuven, Belgium
- Nader FH (2014) The geology of Lebanon. Scientific Press Ltd, United Kingdom, p. 108
- Nader FH, Swennen R (2004) Petroleum prospects of Lebanon: some remarks from sedimentological and diagenetic studies of Jurassic carbonates. *Mar Pet Geol* 21:427–441
- Naylor D, Al-Rawi M, Clayton G, Fitzpatrick MJ, Green PF (2013) Hydrocarbon potential in Jordan. *J Pet Geol* 36(3):205–236
- Needham, D., Hosler, J., Nowak, S., Christensen, C., Ffrench, J., 2013. The Tamar Field from discovery to production (Abstract). AAPG Search and Discovery Article #90161©2013 AAPG European Regional Conference, Barcelona, Spain, 8–10 April 2013
- Netzeband GL, Gohl K, Hubscher CP, Ben-Avraham Z, Dehghani GA, Gajewski D, Liersch P (2006) The Levantine Basin crustal structure and origin. *Tectonophysics* 418:167–188
- Noeth S, Karg H, Littke R (2001) Reconstruction of Late Paleozoic heat flows and burial histories at the Rhenohercynian-Subvariscan boundary, Germany. *Int J Earth Sciences* 90:234–256
- Noeth S, Thomsen RO, Littke R (2002) A method for assessing statistical significance and uncertainties for calibration of 1-D thermal basin maturation models. *AAPG Bull* 86(3):417–431
- OAPEC Annual Report, 2002. Secretary General's Annual Report—Organization of Arab Petroleum Exporting Countries, 29, pp. 229
- Ponikarov VP (1966) The geology of Syria. In: In: Explanatory notes on the geological map of Syria, scale 1:200 000. Ministry of Industry, Syrian Arab Republic
- Powell JH, Moh'd BK (2011) Evolution of Late Cretaceous to Eocene alluvial and carbonate platform sequences in Jordan. *GeoArabia* 17(3):29–82
- Renouard G (1955) Oil prospects of Lebanon. *Am Assoc Pet Geol Bull* 39(11):2125–2169
- Robertson, A.H.F., 1998. Mesozoic - tertiary tectonic evolution of the Easternmost Mediterranean area; integration of marine and land evidence. In: Robertson, A.H.F., Emeis, K.C., Richter, K.C., Camerlenghi, A. (Eds.), Proceedings of the Ocean Drilling Program, Scientific Results, 160, 723–782
- Roded R, Shalev E, Katoshevski D (2013) Basal heat-flow and hydrothermal regime at Golan-Ajloun hydrological basins. *J Hydrol* 476:200–211
- Sachse VF, Littke R, Heim S, Kluth O, Schober J, Boutib L, Jabour H, Perssen F, Sindern S (2011) Petroleum source rocks of the Tarfaya Basin and adjacent areas. *Morocco Org Geochem* 42:209–227
- Saint-Marc P (1972) Le Crétacé inférieur et moyen du bord occidental du Jabal-Sannine (Liban). *Notes et Mémoires sur le Moyen-Orient* 13: 217–226
- Saint-Marc P., 1974.—Étude stratigraphique et micropaléontologique de l'Albien, du Cénomanien et du Turonien du Liban. *Notes et Mémoires sur le Moyen-Orient* 13, 342
- Schenk HJ, Horsfield B, Krooß B, Schaefer RG, Schwochau K (1997) Kinetics of petroleum formation and cracking. In: Welte DH et al. (eds) Petroleum and Basin Evolution. Springer, Berlin 535 pp
- Schütz F, Förster HJ, Förster A (2014) Thermal conditions of the central Sinai Microplate inferred from new surface heat-flow values and continuous borehole temperature logging in central and southern Israel. *J Geodyn* 76:8–24
- Segev A, Rybakov M, Lyakhovsky V, Hofstetter A, Tibor G, Goldshmidt V, Ben Avraham Z (2006) The structure, isostasy and gravity field of the Levant continental margin and the southeast Mediterranean area. *Tectonophysics* 425:137–157
- Shalev E, Lyakhovsky V, Weinstein Y, Ben-Avraham Z (2013) The thermal structure of Israel and the Dead Sea fault. *Tectonophysics* 602: 69–77
- Taylor GH, Teichmüller M, Davis A, Diessel CFK, Littke R, Robert P (1998) Organic petrology. Borntraeger, Stuttgart, p. 704
- Ukla S (1970) Subsurface geology and well correlation in North and Central Lebanon. Master's thesis. American University of Beirut, Lebanon, p. 125
- Villinski, J., 2013. Unusual but effective petroleum systems—disseminated terrestrial organic matter of the upper Oligocene as the primary source rock, offshore Nile delta, Egypt. AAPG Search and Discovery Article #90161©2013 AAPG European Regional Conference, Barcelona, Spain, 8–10 April 2013
- Walley CD (1998) Some outstanding issues in the geology of Lebanon and their importance in the tectonic evolution of the Levantine region. *Tectonophysics* 298:37–62
- Wilson, M., 1992. Magmatism and continental rifting during the opening of the South Atlantic Ocean: a consequence of Lower Cretaceous super-plume activity. In: B. C. Storey, T. Alabaster and R. J. Pankhurst (Eds.), Magmatism and the causes of continental break-up. *Geol. Soc. Lond., Spec Publ*, 68, 241–255
- Wygrala, B.P., 1989. Integrated study of an oil field in the southern Po Basin, Northern Italy. PhD thesis, University of Cologne, Germany
- Wygrala, B., Rottke, W., Kornpohl, D., Neumaier, M., Al-Balushi, A., Marlow, L., 2014. Assessment of controlling factors in mixed biogenic and thermogenic petroleum systems—a case study from the Levantine Basin. Search and Discovery Article #10636, AAPG Annual Convention and Exhibition, Houston, Texas, April 6–9, 2014
- Zilberman E, Calvo R (2013) Remnants of Miocene fluvial sediments in the Negev Desert, Israel, and the Jordanian Plateau: evidence for an extensive subsiding basin in the northwestern margins of the Arabian plate. *J Afr Earth Sci* 82:33–53